JOURNAL OF PETROLOGY | VOLUME 50 | NUMBER 10 | PAGES 1973–1991 | 2009 | doi:10.1093/petrology/egp064

Metamorphism of High/ultrahigh-pressure Pelitic–Felsic Schist in the South Tianshan Orogen, NW China: Phase Equilibria and *P–T* Path

CHUNJING WEI[1]*, WEI WANG[1,2], GEOFFREY L. CLARKE[2], LIFEI ZHANG[1] AND SHUGUANG SONG[1]

[1]MOE KEY LABORATORY OF OROGENIC BELTS AND CRUSTAL EVOLUTION, SCHOOL OF EARTH AND SPACE SCIENCES, PEKING UNIVERSITY, BEIJING 100871, CHINA

[2]SCHOOL OF GEOSCIENCES, UNIVERSITY OF SYDNEY, SYDNEY, NSW 2006, AUSTRALIA

RECEIVED FEBRUARY 4, 2009; ACCEPTED AUGUST 18, 2009

The South Tianshan high/ultrahigh-pressure (HP–UHP) metamorphic belt, NW China is characterized by extensive pelitic–felsic schists with numerous blocks of eclogite, ultramafic rock and marble. The pelitic–felsic schists preserve two generations of garnet-bearing mineral assemblages: (1) an early generation that involves garnet, phengite, glaucophane, and quartz/coesite with or without paragonite; (2) a late generation that involves albite, hornblendic amphibole, quartz and grossular-rich, pyrope-poor garnet. Early generation garnet has growth zoning involving core to rim increases in pyrope content, coupled with increased or constant grossular content. Pseudosection modeling of these growth zoning textures in three samples (T311, T314, and T316) reflects prograde paths and peak conditions of c. 32 kbar at 550–570°C, c. 22.5 kbar at 550°C, and c. 22–23 kbar at 540–550°C, respectively. These P–T estimates are consistent with those recovered from eclogite blocks hosted by the schists. Phase equilibrium modeling predicts that the early garnet would have mainly grown in mineral assemblages involving lawsonite, jadeite and chloritoid, with or without coesite or carpholite, distinct from the assemblages now in the matrix. The post-peak decompression of the pelitic–felsic schists is inferred to have involved two stages. The early stage decompression is characterized by dehydration reactions involving lawsonite and carpholite at $P > 20$ kbar, coupled with mode and compositional changes of garnet, glaucophane and phengite. The late-stage decompression after lawsonite disappearance led to the rocks being fluid-absent. Under such fluid-absent conditions, the solid transition of jadeite to albite occurs at $P \approx 14$ kbar, and hornblendic amphibole forms at 12–13 kbar. Most garnet grains are somewhat changed in composition, to produce a pyrope-poor and grossular-rich outer rim. In contrast to above-solidus conditions, decompression of the pelitic–felsic schists at subsolidus conditions does not destabilize phengitic muscovite and tends to preserve their peak mineral assemblages if there is no intensive fluid infiltration. In the South Tianshan belt, buoyancy of subducted metasediments with respect to mantle rocks could be one of the major reasons for fast exhumation of the HP–UHP rocks.

KEY WORDS: *HP–UHP metamorphism; pelitic–felsic schist; phase equilibria; P–T pseudosection; South Tianshan*

INTRODUCTION

High-pressure accretionary terranes related to oceanic subduction are generally dominated by felsic rocks consisting of quartz, albite, phengitic and paragonitic mica and glaucophane with or without garnet and/or epidote; for example, in Oman (El-Shazly & Liou, 1991), the Seward Peninsula (Thurston, 1985; Patrick & Evans, 1989), South Sulawesi, Indonesia (Miyazaki *et al.*, 1996) and North Qilian, NW China (Wei & Song, 2008). These felsic rocks

*Corresponding author. Telephone: 86-10-62754157. Fax: 86-10-62751159. E-mail: cjwei@pku.edu.cn

may have a greywacke precursor and commonly contain mafic eclogite blocks and pelitic interlayers. Mineral assemblages in the pelitic rocks, involving some typical parageneses (e.g. glaucophane + chloritoid, chloritoid + talc and carpholite + garnet), as well as in the mafic eclogites reflect low-*T*, high-*P* conditions within the jadeite stability field (Miyazaki *et al.*, 1996; Warren & Waters, 2006; Song *et al.*, 2007; Wei & Song, 2008). However, the albite-rich felsic rocks are commonly poorly studied because of their high-variance assemblages and a lack of available geothermobarometric techniques. *P*–*T* estimates for the pelitic and felsic compositions apparently contradict the extensive distribution of albite and the absence of jadeite in the felsic rocks (El-Shazly, 2001). Wei & Powell (2004, 2006) tried to elucidate the phase relations for the felsic rocks in the NKFMASH and NCKFMASH systems, but this work lacked sophisticated mixing models for phases such as amphibole and pyroxene. With more recent advancement of the mixing models for amphibole (Diener *et al.*, 2007) and clinopyroxene (Green *et al.*, 2007) it is feasible to calculate phase equilibria in geologically more realistic systems (such as Na_2O–CaO–K_2O–FeO–MgO–Al_2O_3–SiO_2–H_2O–TiO_2–O, NCKFMASHTO) to examine the metamorphic evolution of rocks poorly addressed by conventional geothermobarometry (e.g. Powell *et al.*, 1998).

The high/ultrahigh-pressure (HP–UHP) belt within the South Tianshan orogen, NW China, is similar to other HP terranes in that it contains blocks of eclogite, marble and serpentinite hosted within extensive pelitic–felsic schists that have received little attention. Through the last decade, the eclogites have been studied by many geologists (e.g. Gao *et al.*, 1999; Zhang *et al.*, 2000, 2002*a*, 2005; Klemd *et al.* 2002; Gao & Klemd, 2003; Wei *et al.*, 2003; Lin & Enami, 2006). Peak *P*–*T* conditions recovered from the eclogite assemblages using various approaches are in the range of 500–600°C and 14–28 kbar. The presence of coesite pseudomorphs, quartz and coesite exsolution lamellae in omphacite, and magnesite (Zhang *et al.*, 2002*a*, 2002*b*, 2005) indicates that at least some of the eclogites reached UHP conditions. Zhang *et al.* (2003) inferred a very high pressure of *c.* 50 kbar at 560–600°C on the basis of magnesite and calcite inclusions in dolomite from a metapelite in the west Muzaert area. Lü *et al.* (2008) reported inclusions of coesite and pseudomorphs after coesite in garnet from the pelitic schists in the east Habutengsu area, consistent with pressures of 27–33 kbar at 570–630°C. Using the pseudosection approach in the NCKFMASH system, Wei & Powell (2006) obtained *P*–*T* conditions of 14·5–16·5 kbar and 600–650°C for a representative felsic rock (AK07) with a mineral assemblage involving garnet, glaucophane, phengite, albite and quartz. Although this *P*–*T* estimate is in accordance with the presence of albite, it is not clear whether garnet and phengite compositionally equilibrated with albite.

Hence, the two objectives in this paper are: (1) to describe the petrography and mineralogy of representative pelitic–felsic schist samples from the South Tianshan orogen; (2) to interpret the phase relations and metamorphic evolution of the pelitic–felsic schists using a pseudosection approach in the NCKMnFMASHO system.

GEOLOGICAL SETTING

The Chinese Tianshan orogen stretches east–west for *c.* 1500 km, separating the Junggar plate to the north and the Tarim plate to the south. It is believed that the Tianshan orogen was formed in the Late Paleozoic during the tectonic amalgamation of the Tarim, Junggar and Yil–Central Tianshan plates, and that the Tertiary collision between India and Eurasia played an important role in reactivating the ancient tectonic structures (Coleman, 1989; Windley *et al.*, 1990; Allen *et al.*, 1992; Gao *et al.*, 1995, 1998).

Windley *et al.* (1990) and Allen *et al.* (1992) recognized two suture zones in the Chinese western Tianshan orogenic belt: the Late Devonian–Early Carboniferous South Tianshan suture zone, which marks the border of the Tarim and Yili–Central Tianshan plates, and the Late Carboniferous–Early Permian North Tianshan suture zone, which marks the boundary between the Yili–Central Tianshan plate and the North Tianshan island arc in the Junggar plate (see Fig. 1a). An elongate, pod-shaped HP–UHP belt is distributed along the South Tianshan suture zone for *c.* 200 km within China. It may be correlated with the Atbashi eclogite belt in the South Tianshan area of Kirghizia (Sobolev *et al.*, 1986; Tagiri *et al.*, 1995) and the Fan–Karategin blueschist belt in the South Tianshan area of Tajikistan (Volkova & Budanov, 1999). The South Tianshan HP–UHP belt in China is mainly composed of felsic–pelitic schists that enclose lenses and blocks of eclogite, ultramafic rock and marble (see Fig. 1b). Trace and rare earth element (REE) characteristics of the eclogites indicate mid-ocean ridge basalt (MORB) to ocean island basalt (OIB) affinities (Gao & Klemd, 2003; Ai *et al.*, 2005). Thus, the HP–UHP belt is inferred to constitute a subduction complex within an accretionary wedge, developed along an active continental margin similar to those of the 'Cordilleran-type' HP–LT rocks formed by subduction of oceanic crust (Maruyama *et al.*, 1996). Gao & Klemd (2003) obtained two Sm–Nd isochron ages of 343 ± 44 Ma and 346 ± 3 Ma from the eclogites, and two $^{40}Ar/^{39}Ar$ plateau ages of 344 ± 1 Ma for crossite and 331 ± 2 Ma for phengite from blueschists. They concluded that the HP rocks were formed by the subduction of a Paleozoic 'South Tianshan Ocean' at *c.* 344 Ma, then exhumed to shallower crustal levels during the collision of the Tarim and Yili–Central Tianshan plates

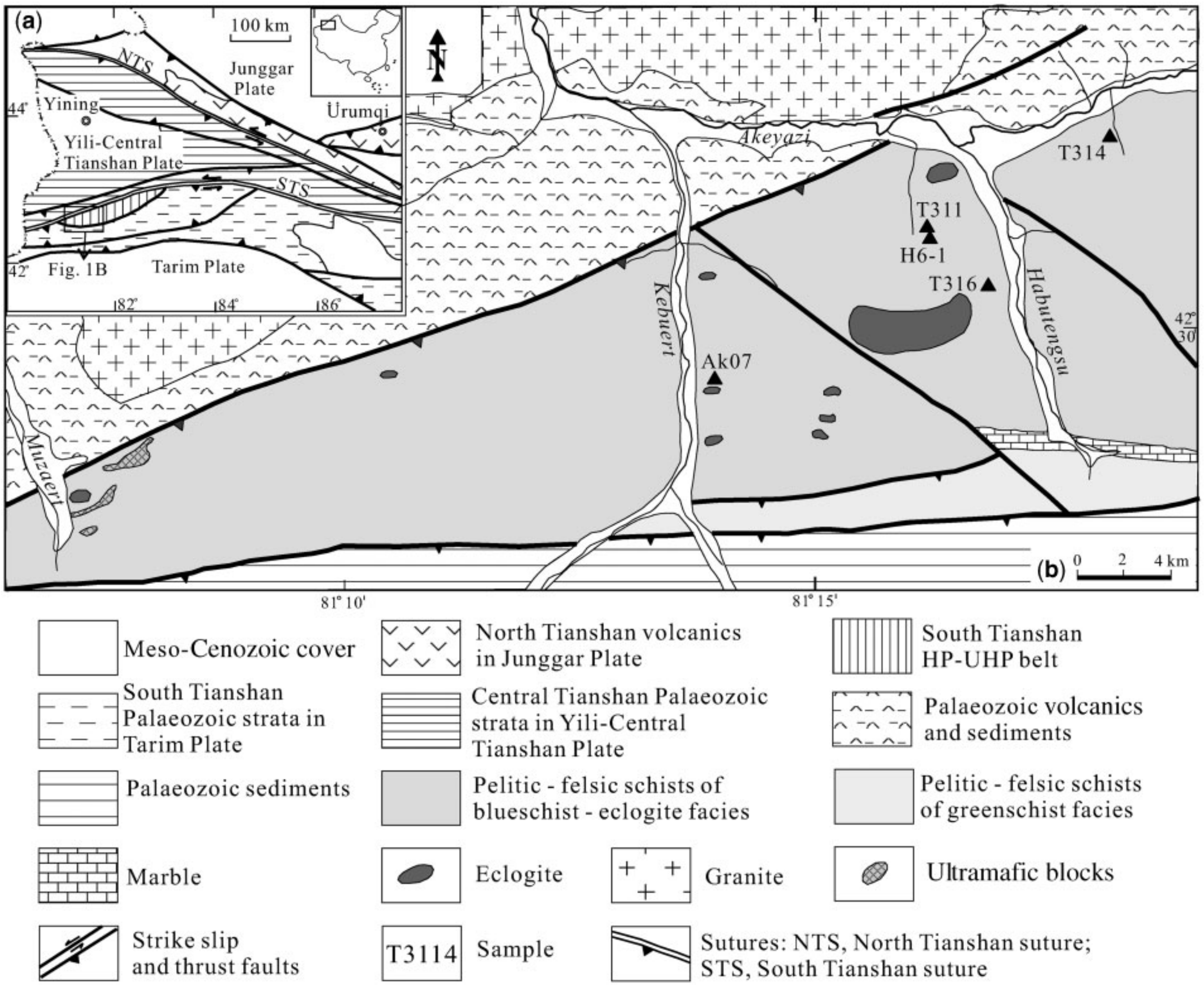

Fig. 1. (a) Tectonic framework of the western part of the Chinese Tianshan orogen; (b) schematic geological map of the South Tianshan HP–UHP belt showing the distribution of eclogite and ultramafic blocks and sample localities.

c. 331 Ma. In the context of ambiguous Sm–Nd and $^{40}Ar/^{39}Ar$ dates for low-*T* and high-*P* rocks (i.e. Kelly *et al.*, 1994; Li *et al.*, 1994; Jahn *et al.*, 2005), Zhang *et al.* (2007) obtained more confirmative sensitive high-resolution ion microprobe (SHRIMP) zircon U–Pb ages of 233 ± 4 to $226 \pm 4{\cdot}6$ Ma from four eclogite samples, consistent with Triassic HP–UHP metamorphism.

To the north of the HP–UHP belt is a high-grade metamorphic belt that consists of garnet–sillimanite gneiss, biotite–plagioclase gneiss, amphibolite, and a typical low-*P* granulite assemblage that includes cordierite. There are also extensive Paleozoic tonalitic–granitic intrusive rocks, Late Silurian–Early Carboniferous volcanic rocks, and some Middle Carboniferous–Late Permian neritic carbonates and clastic rocks in the high-grade belt. Li & Zhang (2004) published a SHRIMP zircon U–Pb age of 280–290 Ma for the low-*P* granulites. It is most likely that this high-grade belt formed part of the active Paleozoic continental margin, paired with the subduction–accretionary complex now evident in the HP–UHP metamorphic belt (Gao *et al.*, 1998; Zhang *et al.*, 2007).

To the south of the HP–UHP belt is a series of southern Tianshan nappes that consist mainly of Silurian–Ordovician carbonates and flysch of low metamorphic grade, overthrust from south to north on a large scale. The HP–UHP belt is separated from the high-grade belt to the north and low-grade belt to the south by large-scale ductile shear zones.

PETROGRAPHY AND MINERAL CHEMISTRY

Three pelitic–felsic schists were selected from more than 50 samples for detailed studies of their petrography and composition. Mineral and whole-rock X-ray fluorescence (XRF) analyses were obtained at the MOE Key

Laboratory of Orogenic Belts and Crustal Evolution of Peking University. The minerals were analyzed using a JXA-8100 microprobe in wavelength-dispersive mode with 15 kV acceleration potential and 10 nA beam current. Matrix corrections were carried out using the PRZ correction program supplied by the manufacturer. Representative microprobe analyses for the three samples are presented in Tables 1–3.

Sample T311

This rock is a garnet–glaucophane–mica schist composed of garnet (12 vol. %), glaucophane (8%), hornblendic amphibole (5%), phengitic muscovite (18%), paragonite (5%), epidote (2%), albite (6%), quartz (42%) and a small amount of rutile, ilmenite and apatite. The modal proportion of paragonite was estimated from backscattered electron images.

Garnet in sample T311 mostly occurs as porphyroblasts and is euhedral to subhedral with a grain size ranging from 0·5 to 1·0 mm across (Fig. 2a). It contains sparse inclusions of quartz, phengite, rutile and apatite. Some quartz inclusions are polycrystalline (Fig. 2b), or with radial fractures (Fig. 2c), probably being pseudomorphs after coesite. The analyzed garnet grain shows a clear zonation where X_{py} [$= Mg/(Mg + Fe + Mn + Ca)$] increases from 0·08 in the core to 0·20–0·23 in the rim, as X_{sps} [$= Mn/(Mg + Fe + Mn + Ca)$] decreases from core to rim (see Fig. 3), showing a pronounced 'bell-shaped profile' (after Spear, 1993). X_{alm} [$= Fe/(Mg + Fe + Mn + Ca)$] increases from the core to the mantle portions of garnet, and then decreases at the grain rim. X_{grs} [$=Ca/(Mg + Fe + Mn + Ca)$] is almost constant from core to rim with a value of 0·07–0·08. A garnet grain enveloped by glaucophane has similar X_{grs} to the garnet porphyroblasts but higher X_{py} (0·26) at the grain rim (R3 in Fig. 2d and Table 1). This garnet, which is relatively poor in grossular and rich in pyrope, is similar to that with coesite inclusions (Fig. 4) described by Lü *et al.* (2008). At the outermost rim (less than 10 μm in width), garnet sometimes has distinct compositions involving lower $X_{py} = 0·08–0·10$ and higher $X_{grs} = 0·26–0·27$ (see RL in Figs 2a, 3 and 4, and Table 1).

Glaucophane is very coarse-grained, with a grain size of 5–6 mm long and 2–3 mm wide. It contains numerous inclusions of garnet, muscovite and rutile, and usually develops a hornblendic amphibole rind 0·2–0·4 mm thick (Fig. 2d). Glaucophane has $X(gl)$ [$=Fe/(Mg + Fe)$] $= 0·36–0·41$, and $\mathcal{Z}(gl)$ ($=Na_{M4}/2$) $= 0·96–0·82$. Some glaucophane grains have weak zonation with $\mathcal{Z}(gl)$ and Si decreasing from core to rim. Hornblendic amphibole occurs as rinds around glaucophane or as a symplectite with albite; the former is mostly katophorite in composition (Leake *et al.*, 1997), and the latter is barroisite (Fig. 5). Phengitic muscovite has Si contents mostly in the range 3·36–3·41 per formula unit (p.f.u.), but muscovite grains close to paragonite have lower Si of 3·31 p.f.u. (Table 1). Albite is chemically close to the pure end-member, generally anhedral and forms grains 0·5–1·5 mm across. Some albite occurs in fine-grained symplectitic intergrowths with hornblendic amphibole. Epidote or clinozoisite has $Fe^{3+}/(Fe^{3+} + Al) = 0·10$.

Sample T314

This rock is a garnet–glaucophane–albite schist composed of garnet (18 vol. %), glaucophane (12%), albite (25%), hornblendic amphibole (2%), phengitic muscovite (2%), paragonite (8%), quartz (26%) and a small amount of rutile and sphene. Secondary chlorite occurs both parallel to and cutting the penetrative foliation.

Garnet in T314 is euhedral with grains 1–3 mm in diameter that are visibly zoned. The measured garnet grain (Fig. 2f) has $X_{py} \approx 0·05$ at the grain core, increasing to *c.* 0·12 at the grain rim. X_{grs} increases from 0·09–0·10 at the core to 0·17–0·19 at the grain rim. X_{sps} decreases from core to rim, and X_{alm} changes only subtly between 0·70 and 0·75. The garnet grain is also characterized by pyrope-poor and grossular-rich ($X_{py} \approx 0·06$, $X_{grs} = 0·24–0·25$) compositions in some parts of its outer rim, which is less than 10 μm in width (RL in Figs 2f, 3 and 4, and Table 2). Garnet has numerous inclusions of quartz, paragonite, epidote, chloritoid, chlorite, and also grossular-rich garnet (Fig. 2g and h). Chloritoid inclusions in garnet have high $X_{Fe} = Fe/(Mg + Fe) = 0·86–0·87$ (see Wei & Song, 2008). Chlorite inclusions in garnet also have higher $X_{Fe} = 0·80–0·64$, and are chemically distinct from chlorite in the rock matrix with $X_{Fe} = 0·45–0·47$. A grossular-rich garnet inclusion has $X_{grs} = 0·41$ and $X_{py} = 0·06$, distinct from other garnet compositions (Fig. 4, and g-In in Fig. 2h and Table 2). As shown in Fig. 2h, Fe-rich chlorite, zoisite/epidote and grossular-rich garnet that occur together probably represent the products of lawsonite breakdown, together with other ferromagnesian minerals such as chlorite. Glaucophane has $X(gl) = 0·34–0·45$ and $\mathcal{Z}(gl) = 0·91–0·99$. The hornblendic amphibole overgrows glaucophane or occurs as intergranular crystals. It has $X(hb) = 0·46–0·47$ and $\mathcal{Z}(hb) = 0·48–0·49$, being barroisite and katophorite. Phengitic muscovite has $Si = 3·26–3·28$. Epidote or clinozoisite has $Fe^{3+}/(Fe^{3+} + Al) = 0·10$. Albite occurs as anhedral poikiloblasts with grain size of 1–3 mm, with numerous inclusions of glaucophane, paragonite and rutile (Fig. 2e).

Sample T316

This rock is a garnet–glaucophane–albite schist composed of garnet (10 vol. %), glaucophane (16%), albite (40%), hornblendic amphibole (8%), phengitic muscovite (7%), paragonite (3%), epidote (3%), quartz (12%) and a small amount of rutile, sphene, chlorite and calcite.

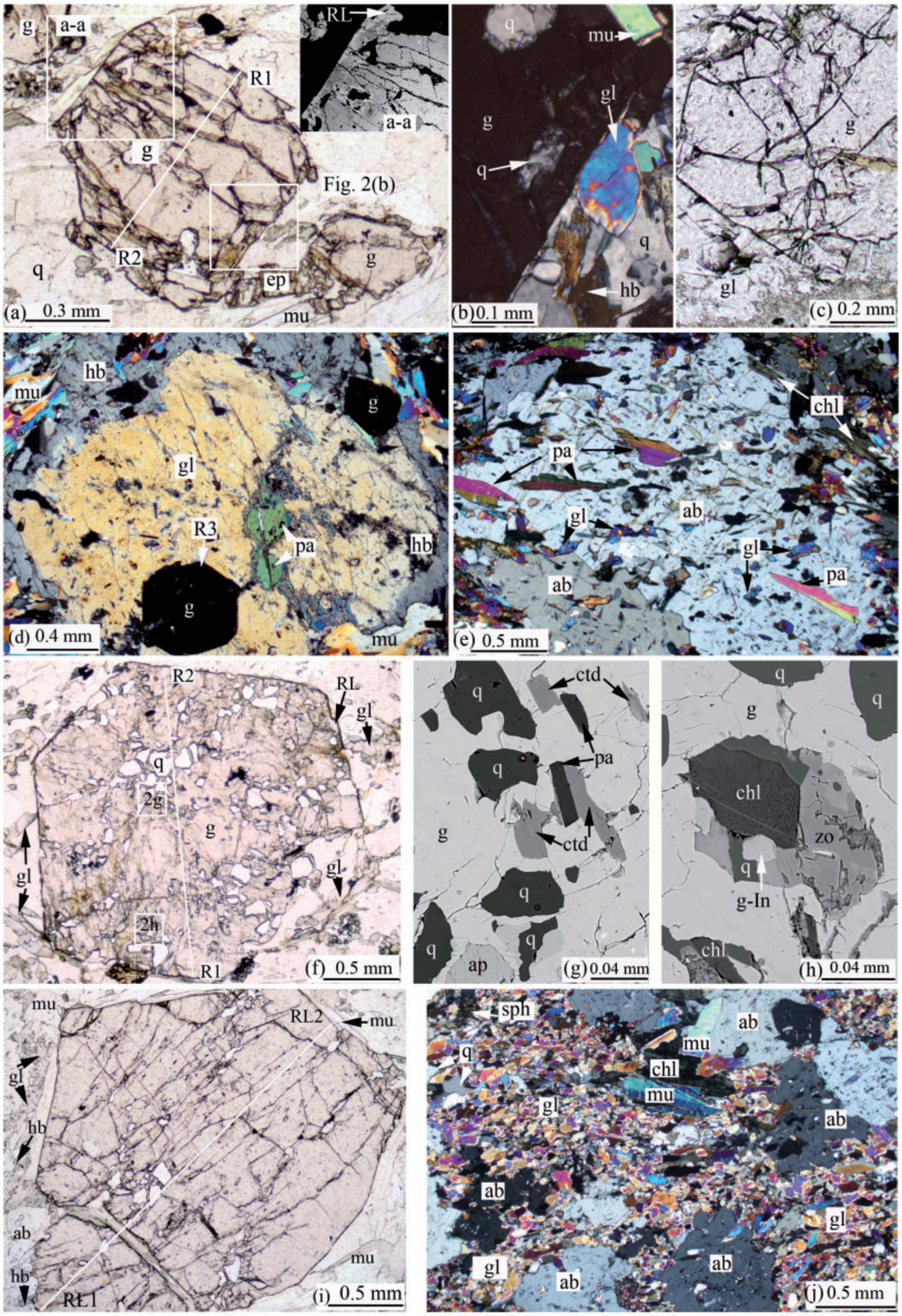

Fig. 2. Photomicrographs and backscattered electron images showing textural relationships in the pelitic–felsic schists, South Tianshan HP–UHP belt. (a) A subhedral garnet grain in sample T311 indicating the location of the zoning profile (R1–R2) shown in Fig. 3 (plane-polarized light). The inserted backscattered electron image (a–a) shows the difference in garnet rim compositions where the dark grey color represents the pyrope-rich and grossular-poor compositions such as R1 and R2, and the light grey color shows the pyrope-poor and grossular-rich compositions such as RL in Table 1. (b) Cross-polarized light photomicrograph showing a polycrystalline quartz inclusion in the garnet grain shown in Fig. 1a. (c) Garnet (sample T311) with a quartz inclusion surrounded by radial fractures, implying a pseudomorph after coesite. (d) A large glaucophane grain (sample T311) with a corona of hornblendic amphibole and a garnet inclusion. R3 refers to the rim composition corresponding to that in Table 1 (cross-polarized light). Paragonite occurs along cracks within the grain. (e) Large albite porphyroblasts with oriented inclusions of glaucophane, paragonite and rutile in sample T314 (cross-polarized light). (f) A garnet grain in sample T314 with numerous inclusions of quartz. The white line R1–R2 shows the location of the zoning profile in Fig. 3 and RL shows the location for the pyrope-poor and grossular-rich analysis in Table 1 (plane-polarized light). (g, h) Backscattered electron images showing inclusions of quartz, chloritoid, paragonite, chlorite, zoisite (epidote), apatite and grossular-rich garnet (g-In) in the garnet (f). (i) A subhedral garnet porphyroblast with a few inclusions of quartz (sample T316). The white line RL1–RL2 shows the zoning profile location in Fig. 3 (plane-polarized light). (j) Cross-polarized light photomicrograph shows inclusion-rich albite in a matrix consisting of glaucophane, phengitic muscovite, hornblendic amphibole, sphene and chlorite (sample T316). ab, albite; ap, apatite; chl, chlorite; ctd, chloritoid; ep, epidote; g, garnet; gl, glaucophane; hb, hornblendic amphibole; mu, phengitic muscovite; pa, paragonite; sph, sphene; zo, zoisite.

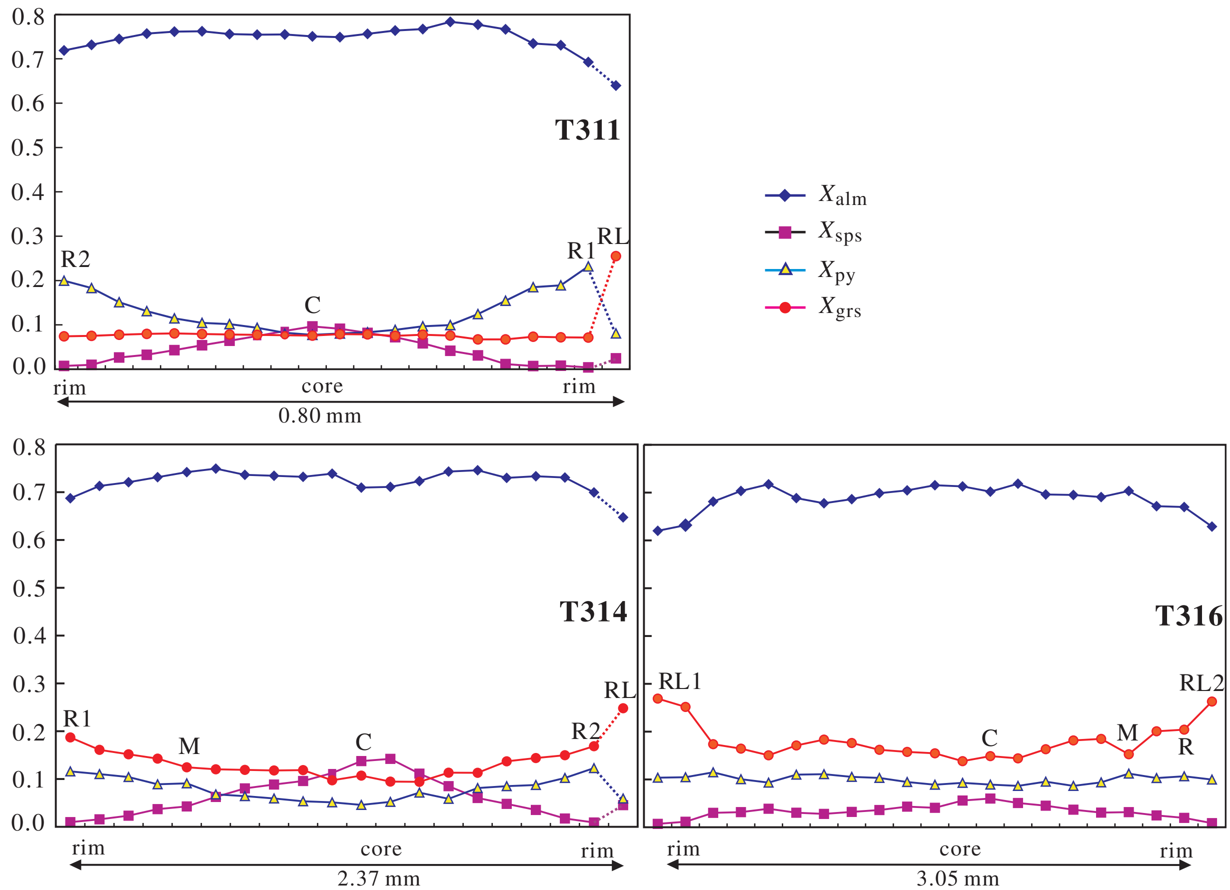

Fig. 3. Zoning profiles of $X_{alm} = Fe^{2+}/(Fe^{2+} + Mn + Mg + Ca)$, $X_{sps} = Mn/(Fe^{2+} + Mn + Mg + Ca)$, $X_{grs} = Ca/(Fe^{2+} + Mn + Mg + Ca)$ and $X_{py} = Mg/(Fe^{2+} + Mn + Mg + Ca)$ through garnet grains in samples T311, T314 and T316, South Tianshan HP–UHP belt. Labels C, M, R, etc. correspond to those in Tables 1–3 and in Figs 6–8.

Garnet in sample T316 has weak zoning involving $X_{py} \approx 0{\cdot}09$ at the grain core, increasing to 0·11–0·12 at the grain mantle and inner rim, and decreasing to *c.* 0·10 at its outer rim. X_{sps} subtly decreases from core to rim, and X_{grs} ranges from 0·14 to 0·18 at the grain core and mantle, subtly increases to *c.* 0·20 at inner rim, and then rapidly increases to 0·25–0·27 (Figs 2i and 3, Table 3) at the grain's outer rim. These grossular-rich and pyrope-poor garnet compositions at the outer rim (of 10–20 µm in width) are similar to those measured in other samples (Fig. 4). Glaucophane occurs as small grains 0·02–0·1 mm long, in agglomerates among albite poikiloblasts (Fig. 2j). It has $X(\text{gl}) = 0{\cdot}40–0{\cdot}46$ and $Z(\text{gl}) = 0{\cdot}92–1{\cdot}00$. Hornblendic amphibole occurs as coronae to glaucophane or as intergranular crystals. It is barroisite or katophorite with $X(\text{hb}) = 0{\cdot}30–0{\cdot}39$, and $Z(\text{hb}) = 0{\cdot}36–0{\cdot}38$. Phengitic muscovite has Si = 3·30–3·32 p.f.u. Epidote or clinozoisite has $Fe^{3+}/(Fe^{3+} + Al) = 0{\cdot}06$. This sample is characterized by the presence of a large proportion of poikiloblastic albite with numerous oriented inclusions of glaucophane, rutile, hornblendic amphibole, paragonite and phengitic muscovite (Fig. 2j).

Whole-rock XRF analyses for the three samples are shown in Table 4. Compositionally, sample T311 is high in Al_2O_3 and K_2O content, close to being a pelite, whereas samples T314 and T316 have an affinity to Na_2O-rich greywacke. Herein, they are referred to as pelitic to felsic schists. Each of them contains two types of amphibole (glaucophane and hornblendic amphibole) and two types of garnet classified simply as grossular-poor and grossular-rich, in addition to phengite, albite and quartz. From a petrographic point of view, all the minerals in each sample could not be grouped into one paragenesis. However, if the grossular-poor garnet, phengitic muscovite and glaucophane are assumed to be of an early paragenesis, the hornblendic amphibole, probably along with the grossular-rich garnet, should be of a later paragenesis. We do not have clear evidence to group albite into one stage. As shown in Fig. 4, the grossular-rich garnet compositions in the later paragenesis for the three samples are similar,

Table 1: Selected microprobe analyses for sample T311 from the South Tianshan HP–UHP belt

Mineral:	g-R1	g-R2	g-R3	g-RL	g-C	gl-C	gl-R	hb	mu-1	mu-2	pa	ep	ab
SiO_2	37·90	37·21	38·53	37·66	36·95	56·14	54·15	46·74	51·71	49·66	46·76	38·92	67·25
TiO_2	—	0·04	—	0·06	0·07	0·01	0·21	0·36	0·26	0·39	0·03	0·15	—
Al_2O_3	22·05	21·93	22·07	21·61	21·28	12·13	12·77	12·57	27·75	29·55	38·66	29·35	19·4
Cr_2O_3	—	0·01	—	0·02	0·02	0·04	0·03	0·04	0·05	—	—	0·03	0·02
FeO	31·54	32·31	30·63	28·18	33·30	10·75	12·16	14·5	2·22	2·32	0·27	4·86	0·07
MnO	0·18	0·32	0·13	1·07	4·21	0·04	0·03	0·03	0·01	—	—	0·09	—
MgO	5·85	4·99	6·68	1·99	1·92	8·88	9·18	9·85	3·30	2·67	0·16	0·03	0·02
CaO	2·51	2·58	2·69	8·76	2·62	0·53	2·14	7·21	—	0·02	0·2	23·69	0·01
Na_2O	—	—	—	—	—	7·79	6·76	4·4	0·74	0·49	7·81	—	0·19
K_2O	—	—	—	—	—	0·01	0·09	0·32	10·19	10·33	0·7	0·02	12·67
Total	100·02	99·39	100·73	99·35	100·37	96·32	97·52	96·02	96·23	95·43	94·59	97·14	99·63
O	12	12	12	12	12	23	23	23	11	11	11	12·5	8
Si	2·98	2·96	2·99	3·00	2·98	7·87	7·57	6·89	3·41	3·31	3·02	3·01	2·98
Ti		0·00		0·00	0·00	0·00	0·02	0·04	0·01	0·02	0·00	0·01	
Al	2·04	2·06	2·02	2·03	2·02	2·00	2·11	2·18	2·16	2·32	2·94	2·68	1·01
Cr		0·00		0·00	0·00	0·00	0·00	0·01	0·00			0·00	0·00
Fe^{3+}	0·00	0·02	0·02	0·00	0·01	0·00	0·14	0·23	0·00	0·00	0·00	0·31	0·08
Fe^{2+}	2·07	2·13	1·96	1·88	2·24	1·26	1·28	1·55	0·12	0·13	0·02	0·00	0·00
Mn	0·01	0·02	0·01	0·07	0·29	0·01	0·00	0·00	0·00			0·01	
Mg	0·69	0·59	0·77	0·24	0·23	1·85	1·91	2·16	0·33	0·27	0·02	0·00	0·00
Ca	0·21	0·22	0·22	0·75	0·23	0·08	0·32	1·14		0·00	0·01	1·96	0·01
Na						2·12	1·83	1·26	0·10	0·06	0·98		1·03
K						0·00	0·02	0·06	0·86	0·88	0·06	0·00	0·00
X(phase)	0·23	0·20	0·26	0·08	0·08	0·40	0·40	0·42					
Y(phase)	0·07	0·07	0·08	0·26	0·08	0·96	0·82	0·40				0·10	

X(g) = Xpy = Mg/(Fe + Mn + Mg + Ca), X(gl, hb) = Fe^{2+}/(Fe^{2+} + Mg). Y(g) = Xgrs = Ca/(Fe + Mn + Mg + Ca), Y(gl, hb) = (Na/(Na + Ca))M4. Y(ep) = Fe^{3+}/(Fe^{3+} + Al^{VI}). G-R1, -R2, -A correspond to labels in Fig. 4; -in, inclusion in garnet, -C, core; -R, rim; —, not analyzed because of low content <0·1%. The mineral formulae were calculated with the program AX (Holland; http://www.esc.cam.ac.uk/astaff/holland/ax.html).

but their core and rim compositions drawn from the early paragenesis are distinct.

PHASE EQUILIBRIA AND *P–T* EVOLUTION

For the mineral assemblages and compositions mentioned above, the model system NCKMnFMASHO [Na_2O–CaO–K_2O–MnO–FeO–MgO–Al_2O_3–SiO_2–H_2O–O (Fe_2O_3)] was chosen to calculate P–T pseudosections for the pelitic–felsic schists from South Tianshan. Quartz and a fluid phase that is assumed to be pure H_2O, are considered to be in excess. TiO_2 was omitted from our calculations because it is mainly present in the most common accessory phases rutile and sphene, and incorporated only in trivial amount in the main silicate minerals (see Tables 1–3). MnO is included as it affects the stability fields of garnet (Wei *et al.*, 2004).

It is critical to generate an appropriate effective bulk composition (Tracy, 1982; Vance & Holland, 1993; Stüwe, 1997) for the phase equilibrium calculations in the chosen model system, because a rock may have had various equilibrium domains, even on the thin-section scale (Powell, 1978). Thus, an XRF analysis for a piece of rock generally cannot be used to model well the phase equilibria observed in a thin-section because of (1) fractionation consequent to the growth of porphyroblasts, commonly evident as zoned minerals, (2) the heterogeneous accumulation of some minerals (e.g. mica-rich folia), and (3) the effect of retrograde metamorphism. There have been several methods for calculating effective bulk compositions mainly related to garnet growth (Marmo *et al.*, 2002; Evans, 2004; Tinkham & Ghent, 2005). The bulk-rock compositions used in our calculation were generated by integrating mineral compositions and modal abundance data for the phases present, where only half of the modal abundance

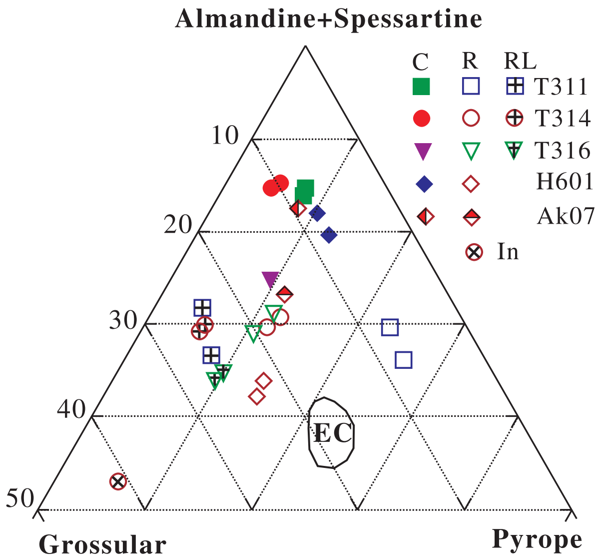

Fig. 4. Ternary diagram with apices almandine + spessartine, grossular and pyrope showing the garnet compositions in the pelitic–felsic schists and their comparison with the garnet in eclogite from the South Tianshan HP–UHP belt (field labelled EC, Wei *et al.*, 2003). Samples H601 and Ak07 are from Lü *et al.* (2008) and Wei & Powell (2004). C, R and RL refer to the analyses at core, rim and outermost rim of garnet grain corresponding to those in Fig. 3 and Tables 1–3. In, grossular-rich garnet inclusion in sample T314.

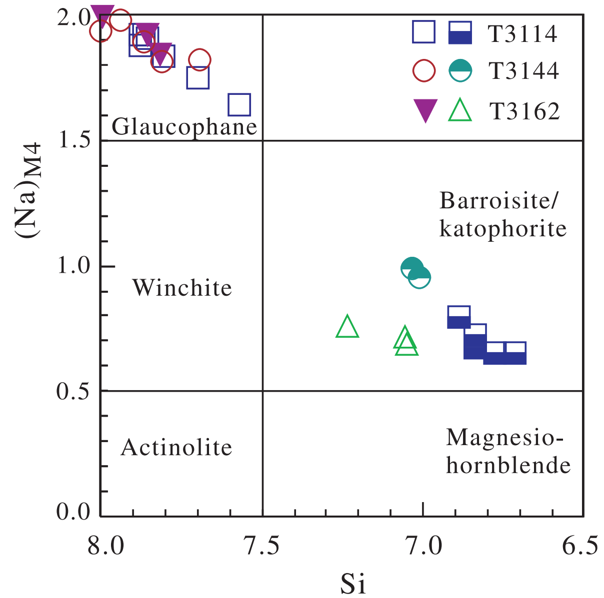

Fig. 5. Si vs $(Na)_{M4}$ p.f.u. diagram showing compositions of amphibole in the pelitic–felsic schists, South Tianshan HP–UHP belt.

of zoned garnet is taken into account (Carson *et al.*, 1999; White *et al.*, 2003; Warren & Waters, 2006). The calculated effective bulk-rock compositions in the model system NCKMnFMASHO are shown in Table 4; these mostly approximate to the XRF analyses. The higher contents of Al_2O_3 in samples T314 and T316 may reflect preferential sampling of textural domains relatively rich in mica and garnet in the preparation of the thin-sections. The bulk-rock compositions generated with this approach are approproate to model the phase equilibria from the pre-peak to the peak stage of metamorphism (Warren & Waters, 2006).

P–T and *P–M*(H_2O) pseudosections are used here to establish the phase relationships of the pelitic–felsic rocks in South Tianshan. As pointed out by Powell & Holland (2008), pseudosections involve a forward calculation of mineral equilibria for a given rock composition. They do not merely give the conditions of formation of a mineral assemblage, and commonly allow sections of *P–T* paths to be deduced from the way that mineral proportions and mineral compositions are interpreted to have evolved during the textural evolution of a rock. *P–M*(H_2O) pseudosections are appropriate to assess evolving mineral assemblages in terms of changes in water content during decompression.

Pseudosection calculations were performed using THERMOCALC 3.30 (Powell *et al.*, 1998, updated July 2006), using the November 2003 updated version of the Holland & Powell (1998) dataset (file tcds55.txt). Activity–composition relationships were updated from those presented for garnet (Wei *et al.*, 2004), epidote (Holland & Powell, 1998), chlorite (Holland *et al.*, 1998), clinopyroxene (Green *et al.*, 2007), amphibole (Diener *et al.*, 2007), paragonite and phengitic muscovite (Coggon & Holland, 2002), biotite (Powell & Holland, 1999), albite (Holland & Powell, 1996), and chloritoid and carpholite (Wei & Powell, 2004). Lawsonite, kyanite, quartz are pure end-member phases.

Pseudosection for a garnet–glaucophane–mica schist (sample T311)

The NCKMnFMASHO *P–T* pseudosection calculated for the garnet–glaucophane–mica schist (sample T311) is presented in Fig. 6a. It is dominated by tri- and quadrivariant fields with a few di- and quini- variant fields that should have been 'witnessed' by the bulk-rock composition. Unfortunately, it does not include a *P–T* field appropriate to the inferred early generation mineral assemblage involving glaucophane, garnet, phengitic muscovite and quartz.

An alternative approach involves recovering *P–T* information recorded by the compositional zoning in garnet. Isopleths of the pyrope and grossular contents in garnet are shown in Fig. 6a, and the core–rim profile C–R1 (Fig. 3) predicts that garnet growth could have occurred along a *P–T* vector from 27·7 kbar at 498°C to 32·4 kbar at 552°C, with the garnet mainly having grown in the mineral assemblage gl–g–jd–car–law–coe. Zoning recorded by the other half of the grain (profile C–R2, Fig. 3) indicates a similar *P–T* vector, but with subtly lower grade peak conditions. The rim composition of the garnet grain enveloped in glaucophane predicts higher

Table 2: Selected microprobe analyses for sample T314 from the South Tianshan HP–UHP belt

Mineral:	g-C	g-R	g-RL	g-In	gl	hb	mu	pa	ctd	chl-m	chl-in	ep	ab
SiO_2	36·85	38·02	37·58	38·37	57·63	48·61	49·41	46·06	24·40	26·66	23·92	39·83	66·96
TiO_2	0·07	0·01	0·09	0·12	—	0·27	0·23	0·05	—	0·02	0·01	0·20	—
Al_2O_3	21·31	21·15	21·36	22·07	11·82	12·88	30·53	38·51	40·99	19·56	21·07	29·73	19·27
Cr_2O_3	0·02	0·05	—	0·03	—	0·02	—	—	0·03	0·01	0·03	0·01	—
FeO	31·09	30·87	28·81	23·21	11·20	12·88	2·19	0·24	24·56	24·73	38·17	4·71	0·07
MnO	5·95	0·43	1·99	0·69	—	0·10	0·10	0·03	0·61	0·08	0·33	—	0·04
MgO	1·13	2·92	1·48	1·54	8·91	8·83	2·51	0·12	2·18	15·65	5·33	0·07	0·02
CaO	3·67	6·55	8·61	14·46	0·09	6·19	0·03	0·11	0·03	0·14	0·02	23·78	0·04
Na_2O	—	—	—	—	8·24	5·00	0·49	8·32	0·02	0·21	0·12	0·03	12·1
K_2O	—	—	—	—	0·02	0·34	10·09	0·41	—	0·11	0·03	—	0·04
Total	100·09	100·01	99·93	100·50	97·91	97·74	95·56	93·85	92·82	87·17	89·03	98·35	98·53
O	12	12	12	12	23	23	11	11	6	14	14	12·5	8
Si	2·98	3·02	3·00	2·99	7·94	7·03	3·28	3·00	1·00	2·82	2·67	3·03	2·98
Ti	0·00	0·00	0·01	0·01		0·03	0·01	0·00		0·00	0·00	0·013	
Al	2·04	1·98	2·01	2·03	1·92	2·20	2·39	2·95	1·99	2·44	2·77	2·67	1·01
Cr	0·00	0·00		0·00		0·00			0·00	0·00	0·00	0·00	
Fe^{3+}	0·00	0·00	0·00	0·00	0·00	0·19	0·02	0·00	0·00	0·00	0·00	0·30	0·00
Fe^{2+}	2·11	2·05	1·92	1·52	1·29	1·69	0·11	0·01	0·85	2·19	3·56	0·00	0·00
Mn	0·41	0·03	0·14	0·05		0·01	0·01	0·00	0·02	0·01	0·03		0·00
Mg	0·14	0·35	0·18	0·18	1·83	1·90	0·25	0·01	0·13	2·47	0·89	0·01	0·00
Ca	0·32	0·56	0·74	1·21	0·01	0·96	0·00	0·01	0·00	0·02	0·00	1·94	0·00
Na					2·20	1·40	0·06	1·05	0·00	0·04	0·03	0·00	1·04
K					0·00	0·06	0·85	0·03		0·02	0·00		0·00
X(phase)	0·05	0·12	0·06	0·06	0·41	0·47			0·86	0·47	0·80		
Y(phase)	0·11	0·19	0·25	0·41	0·99	0·49						0·10	

X(ctd, chl) $= Fe^{2+}/(Fe^{2+} + Mg)$; others are the same as for Table 1.

grade P–T conditions of 32 kbar at 568°C (g-R3, Table 1). Thus, peak conditions for sample T311 can be inferred to have involved $P \approx 32$ kbar and $T = 550$–570°C. The similarity of the garnet compositions between samples T311 and H06-1 (Fig. 4), with the latter containing coesite inclusions in garnet (Lü *et al.*, 2008), and the observed pseudomorphs after coesite in garnet (Fig. 2b and c) support these predictions made using phase equilibria modeling.

Contours of H_2O contents saturated with respect to the mineral assemblages shown in Fig. 6a indicate that the modeled prograde P–T vector cuts isopleths of decreasing H_2O content, reflecting conditions appropriate for the rock having remained fluid-present along the prograde path. Successive mineral assemblages would have evolved through dehydration reactions (Guiraud *et al.*, 2001; Clarke *et al.*, 2006), presenting an optimal case for the inference of equilibrium conditions.

Like those for the South Tianshan eclogites (Klemd *et al.*, 2002; Zhang *et al.*, 2003) and also for the most UHP rocks in the other terranes (Carswell & Zhang, 2000), the post-peak decompression paths for the pelitic–felsic schists are inferred to have been dominated by rapid, nearly isothermal processes, although 'ideal' isothermal decompression is probably not reasonable. For an isothermal process, the mineral assemblage evolution could be well illustrated in the P–X pseudosections. Figure 6b is a P–$M(H_2O)$ pseudosection, which is appropriate to discuss mineral assemblages evolving with variation in H_2O content. As shown in Fig. 6b, a decompression path from the inferred peak condition (P) would deviate from H_2O-saturated conditions and enter the H_2O-absent assemblage gl–g–jd–car–law, assuming that all water released during prograde dehydration had been lost from the rock (Guiraud *et al.*, 2001) and there was no water infiltration. At $P \approx 27$ kbar, the rock would regain H_2O-saturated conditions, and, with further decompression, equilibria would evolve along the H_2O-saturation line to lower $M(H_2O)$. As pressure continues to decrease, mineral assemblage changes predicted by the modeling include (1) glaucophane growth and (2) decreasing modes of carpholite, lawsonite and

Table 3: Selected microprobe analyses for sample T316 from the South Tianshan HP–UHP belt

Mineral:	g-C	g-M	g-R	g-RL2	gl	hb	mu	pa	ep	ab	chl
SiO_2	36·93	38·07	37·74	38·13	55·86	47·9	48·58	47·00	38·85	67·91	26·99
TiO_2	0·05	0·08	0·05	—	—	0·16	0·36	0·06	0·18	0·00	0·01
Al_2O_3	20·32	21·38	21·65	22·2	11·17	10·08	27·96	39·03	31·24	19·29	20·19
Cr_2O_3	0·06	—	0·01	—	0·07	0·04	—	—	—	—	0·01
FeO	32·47	31·63	29·92	28·29	13·31	14·74	2·79	0·15	2·90	0·12	21·83
MnO	2·62	1·4	0·86	0·37	0·09	0·16	0·06	—	—	—	—
MgO	2·21	2·83	2·67	2·52	8·53	11·01	2·71	0·21	0·06	—	18·42
CaO	5·14	5·36	7·11	9·23	0·95	7·86	0·02	0·09	23·44	0·01	0·03
Na_2O	—	—	—	—	7·82	4·14	0·74	7·33	0·03	12·09	—
K_2O	—	—	—	—	0·06	0·33	10·38	0·98	0·01	0·03	0·07
Total	99·84	100·76	100·02	100·75	97·86	96·41	93·61	94·85	96·70	99·45	87·55
O	12	12	12	12	23	23	11	11	12·5	8	14
Si	2·98	3·01	3·00	2·99	7·82	7·05	3·32	3·02	3·00	2·99	2·79
Ti	0·00	0·01	0·00			0·02	0·02	0·00	0·01	0·00	0·00
Al	1·93	1·99	2·03	2·05	1·84	1·75	2·25	2·95	2·84	1·00	2·46
Cr	0·00		0·00		0·01	0·01					0·00
Fe^{3+}	0·10	0·00	0·00	0·00	0·06	0·25	0·00	0·00	0·19	0·00	0·00
Fe^{2+}	2·09	2·09	1·99	1·85	1·50	1·57	0·16	0·01	0·00	0·00	1·89
Mn	0·18	0·09	0·06	0·03	0·01	0·02	0·00				
Mg	0·27	0·33	0·32	0·29	1·79	2·42	0·28	0·02	0·01		2·84
Ca	0·44	0·45	0·61	0·78	0·14	1·24	0·00	0·01	1·94	0·00	0·00
Na					2·12	1·18	0·10	0·91	0·00	1·03	
K					0·01	0·06	0·91	0·08	0·00	0·00	0·01
X(phase)	0·09	0·11	0·11	0·10	0·46	0·39					0·40
Y(phase)	0·15	0·15	0·20	0·26	0·92	0·35			0·06		

Notes are the same as for Tables 1 and 2.

Table 4: Whole-rock compositions of pelitic–felsic schists from the South Tianshan HP–UHP belt (wt%)

Sample	SiO_2	TiO_2	Al_2O_3	Fe_2O_3	FeO	MnO	MgO	CaO	Na_2O	K_2O	P_2O_5	LOI	Total
XRF analyses													
T311	69·33	0·55	12·94	1·11	3·93	0·12	2·24	1·34	1·95	2·91	0·18	2·48	99·08
T314	65·62	0·73	11·85	2·31	7·98	0·23	2·24	2·03	4·90	0·07	0·26	1·35	99·58
T316	62·93	0·54	13·63	2·40	6·20	0·12	3·16	1·34	6·07	0·74	0·17	1·94	99·25
Effective bulk-rock compositions in NCKMnFMASHO calculated from mineral modes and microprobe analyses													
T311	71·08		13·33	0·42	5·28	0·09	2·52	1·42	2·28	2·07		1·50	100·00
T314	64·91		16·13	0·46	7·47	0·07	2·44	2·01	4·84	0·27		1·40	100·00
T316	62·33		17·03	0·76	5·92	0·07	2·89	2·40	6·68	0·80		1·14	100·00

jadeite through successive dehydration reactions. The measured Si = 3·36–3·41 p.f.u. in most phengite is consistent with $P = 25$–27 kbar at $T = 560°C$, which would match phengite recrystallization to this decompression stage. A pronounced step in dehydration is predicted to occur when the carpholite-bearing assemblage was replaced by paragonite-bearing equilibria at $P \approx 24$ kbar. Lower Si contents (3·31 p.f.u.) in phengite occurring with paragonite could reflect continuous changes in phengite composition at this stage. Decompression in the quadrivariant

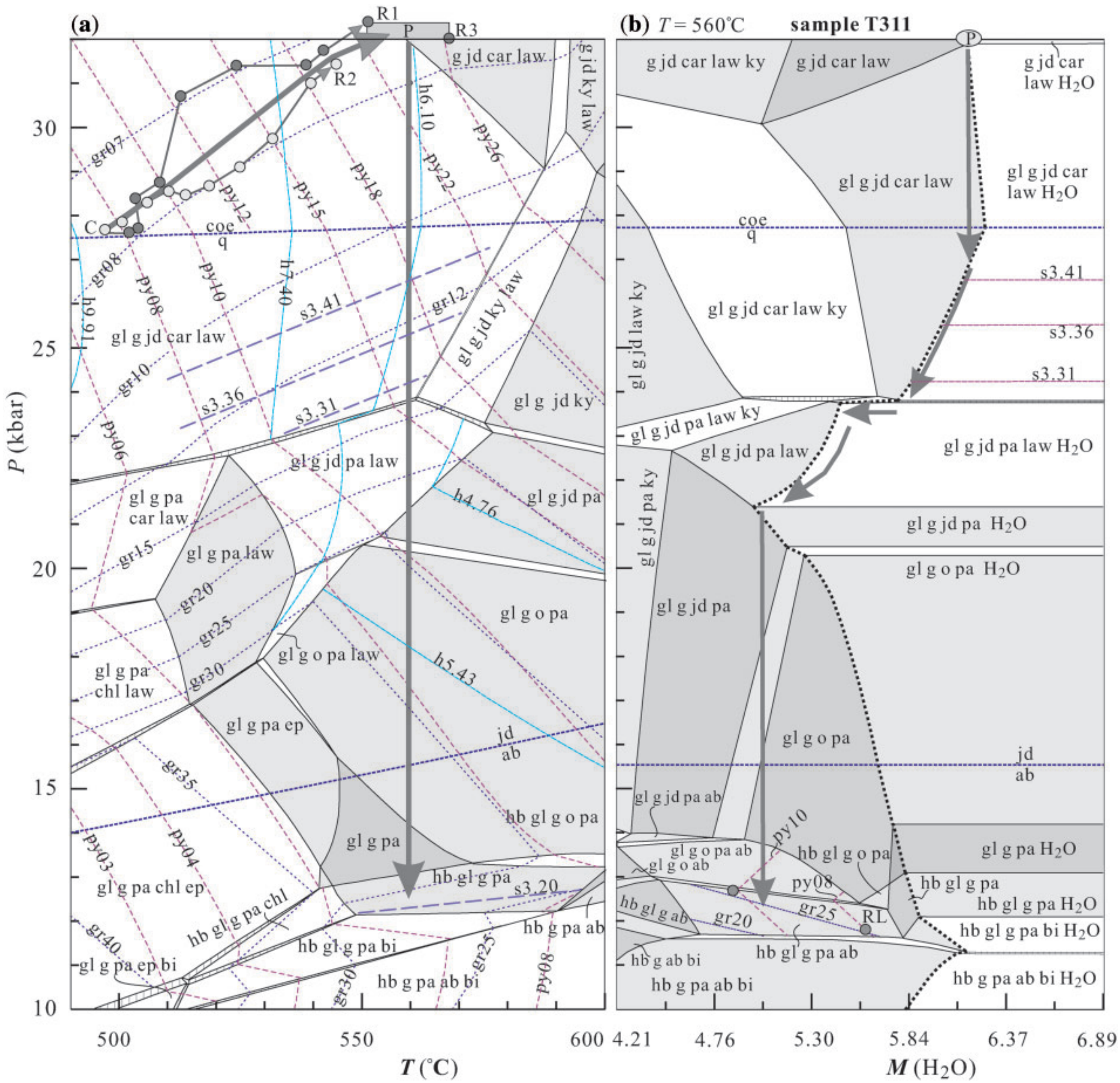

Fig. 6. (a) P–T pseudosection for sample T311 from the South Tianshan HP–UHP belt in the system NCKMnFMASHO (+quartz + phengitic muscovite + H_2O) with a bulk composition calculated on the basis of normalized mole proportions as SiO_2 = 76·64, Al_2O_3 = 8·47, CaO = 1·65, MgO = 4·06, FeO = 5·10, K_2O = 1·42, Na_2O = 2·38, MnO = 0·08, O = 0·20. (b) P–$M(H_2O)$ pseudosection at T = 560°C with quartz and phengitic muscovite, but not H_2O, in excess for sample T311. The trivariant fields are patterned with grey vertical lines, quadrivariant fields are unshaded, quinivariant fields are more lightly shaded, and hexa-variant fields are more darkly shaded. The bold dotted line in (b) refers to the H_2O saturation line. The pseudosections are contoured with isopleths of X_{grs} (gr08–gr40) and X_{py} (py03–py26) in garnet, Si content in phengite (s3·20–s3·41) and H_2O content (h9·91–h4·76) for the corresponding mineral assemblages. The H_2O content refers to $100H_2O/(Na_2O + CaO + K_2O + MnO + FeO + MgO + Al_2O_3 + SiO_2 + H_2O + O$, on a mole basis). Projection of the garnet compositions is shown as dark or light grey circles with the labels C, R1, R2, R3 and RL corresponding to those in Fig. 3 and Table 1. car, carpholite; jd, jadeite; ky, kyanite; law, lawsonite; o, omphacite; other mineral abbreviations are the same as in Fig. 2.

assemblage gl–g–jd–pa–law is also predicted to have involved further dehydration through the replacement of jadeite and lawsonite by glaucophane and paragonite. The limit of H_2O-saturated equilibria has an inflection at $P \approx 21{\cdot}5$ kbar (Fig. 6b) where the rock is predicted to have a H_2O content of 5·03 (mol %)—above or below 21·5 kbar, H_2O-saturated equilibria occur at higher $M(H_2O)$ values. If there was H_2O infiltration to saturate the assemblage with water, further decompression is predicted to be accompanied by an evolutionary path along the H_2O saturation line at conditions involving higher $M(H_2O)$. Changes predicted in the rock include omphacite replacing jadeite at $P \approx 20{\cdot}5$ kbar, and appearance of hornblendic amphibole, biotite and albite at pressures, respectively, of *c.* 13, 12 and 11 kbar. However, this retrograde mineral association has not been observed in the rock. It seems more likely that decompression after lawsonite disappeared was accompanied by water-absent conditions (Fig. 6b). Under such conditions, the appearance of albite either from omphacite or more probably from jadeite would have occurred at $P \approx 14$ kbar, at higher pressures than that for the appearance of albite at H_2O-saturated conditions.

The late-generation garnet compositions with $X_{py} = 0{\cdot}08$–$0{\cdot}10$ and $X_{grs} = 0{\cdot}26$–$0{\cdot}27$ closely match the H_2O-absent assemblage hb–gl–g–pa–ab–(mu + q) at $P = 11{\cdot}8$–$12{\cdot}7$ kbar and $M(H_2O)$ = 4·87–5·61 (mol %). The mineral assemblage observed in sample T311 has a water content of 5·14 mol % consistent with these predicted conditions, and only subtly higher than the $M(H_2O)$ value predicted for lawsonite breakdown.

The compositional variation in the zoned glaucophane crystal in which Z(gl) decreases from 0·96 to 0·82 (core to rim) is in agreement with the values predicted for the decompressional path, but the measured $X(\mathrm{gl}) = 0{\cdot}36$–$0{\cdot}41$ lies closer to values predicted for the H_2O-absent assemblage hb–gl–g–pa–ab–(mu + q). The measured $Z(\mathrm{hb}) = 0{\cdot}15$–$0{\cdot}34$ in the hornblendic amphibole reflects lower pressure conditions.

In summary, compositional zoning in garnet in sample T311 records a progressive metamorphic process at UHP conditions. Paragonite and glaucophane mainly formed during early stage decompression in the stability field of lawsonite. The formation of albite, hornblendic amphibole, and later grossular-rich garnet indicates recrystallization at H_2O-absent conditions at $P = 14$–12 kbar. The Si content in phengite reflects an early stage of the decompression. The main minerals at present forming sample T311 do not reflect an equilibrium state at the inferred peak P–T conditions; they reflect substantial recrystallization along the decompression path.

Pseudosection for a garnet–glaucophane schist (sample T314)

The NCKMnFMASHO P–T pseudosection calculated for the garnet–glaucophane schist (sample T314) is presented in Fig. 7a. This pseudosection is distinguished from the others (Figs 6a and 8a) by the presence of chloritoid-bearing equilibria at $P \approx 21$–25 kbar and $T < 570°$C. Pyrope and grossular zoning measured in the garnet grain can be modeled along a P–T vector from 21·7 kbar at 482°C (point C, Fig. 7a) to maximum P conditions at 23·8 kbar and 526°C (point M, Fig. 7a), and to peak conditions at 22·5 kbar and 553°C (point R, Fig. 7a). Garnet growth would have occurred in the quadrivariant assemblages gl–g–jd–ctd–law and gl–g–jd–pa–law, consistent with the inclusions observed in garnet involving chloritoid, paragonite and the probable lawsonite breakdown-related aggregates consisting of epidote, Fe-rich chlorite and Ca-rich garnet. This prograde P–T path recovered from garnet zoning is characteristic of an increase in both pressure and temperature during the early stage of garnet growth, followed by a continued temperature increase at constant or decreasing pressure conditions. However, it is possible that the prograde P–T vector continued at coupled increasing pressure and temperature conditions to a peak (point P, Fig. 7a) followed by isothermal decompression to the peak conditions (point R, Fig. 7a) recovered from the mineral compositions (as shown by the bold dashed arrow). In this case, garnet compositions in the outer mantle and rim could be interpreted as having been modified by metamorphic reactions in the early decompression stage.

Contouring of the H_2O content saturated with respect to the various mineral assemblages suggests that the probable P–T vector C–M–P (Fig. 7a) would progress to successively lower H_2O contents, and that the mineral assemblage would evolve as the P–T conditions changed. However, isothermal decompression from this probable peak (P) without any fluid ingress would initially place the rock in water-absent conditions (Fig. 7b). A change from carpholite to chloritoid-bearing equilibria at $P \approx 24{\cdot}5$ kbar is coupled with a large step in water content, substantially dehydrating the rock along its modeled decompression path. Further notable dehydration is predicted to occur as chloritoid-bearing assemblages give way to the paragonite-bearing assemblages at $P \approx 23{\cdot}5$ kbar. Continued decompression in the assemblage gl–g–jd–pa–law is still dominated by dehydration reactions, until lawsonite is no longer stable. A prediction from this diagram is that garnet rim compositions should have been affected by these dehydration reactions. When lawsonite was consumed at $P \approx 22{\cdot}6$ kbar, the rock is predicted to have had a H_2O content of 3·83 (mol %). In the absence of water ingress, further decompression is predicted to have occurred in the H_2O-absent assemblage gl–g–jd–pa. At $P \approx 14$ kbar, albite is predicted to replace early jadeite, and hornblendic amphibole predicted to form at $P \approx 12$ kbar. Late-stage garnet in this rock has higher X_{grs} (0·24–0·25) and lower X_{py} (*c.* 0·06) that best match the modeled values in the H_2O-absent assemblage gl–hb–g–pa–ab–bi at $P \approx 11$ kbar and $M(H_2O)$ = 5·44–5·57 (mol %). The mineral assemblage observed in sample T314 has a H_2O content with $M(H_2O) \approx 4{\cdot}83$. Both this H_2O content and the late garnet rim compositions in the context of the modeled mineral equilibria are consistent with some water infiltration into the rock having occurred during the later-stage decompression.

Measured glaucophane and hornblendic amphibole compositions are close to those predicted by the pseudosection (Fig. 7b) at $P = 11{\cdot}8$ kbar and $M(H_2O)$ = 4·80 in the H_2O-absent assemblage hb–gl–g–pa–ab. The Si content

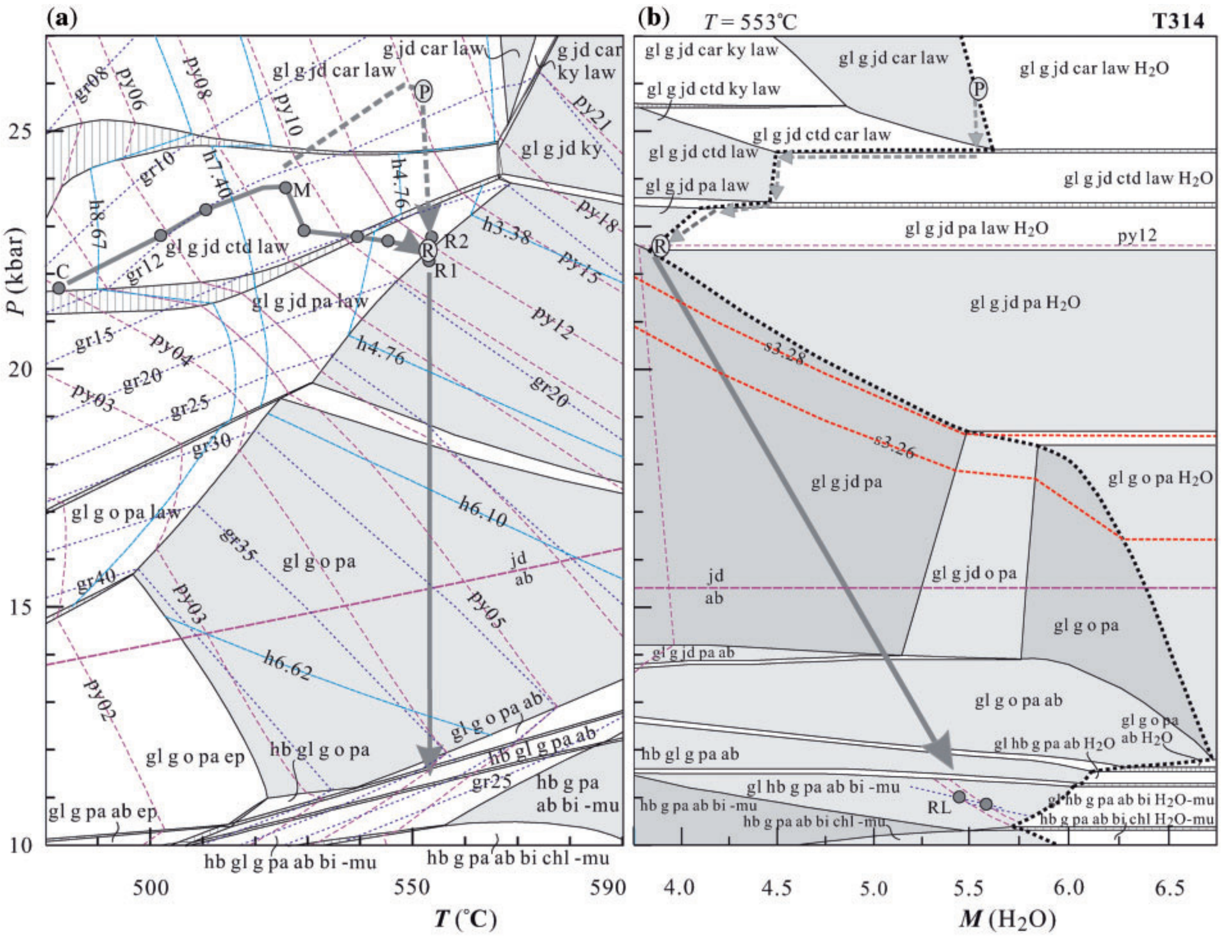

Fig. 7. (a) P–T pseudosection for sample T314 from the South Tianshan HP–UHP belt in the system NCKMnFMASHO (+quartz + phengitic muscovite + H_2O) with a bulk composition calculated on the basis of normalized mole proportions as $SiO_2 = 70{\cdot}64$, $Al_2O_3 = 10{\cdot}34$, CaO = 2·34, MgO = 3·96, FeO = 7·18, $K_2O = 0{\cdot}19$, $Na_2O = 5{\cdot}10$, MnO = 0·07, O = 0·19. (b) P–$M(H_2O)$ pseudosection at $T = 553$°C with quartz and phengitic muscovite in excess for sample T314. The bold dotted line in (b) refers to the H_2O saturation line. Projection of the garnet compositions is shown as dark grey circles with the labels C, M, R1, R2 and RL corresponding to those in Fig. 3 and Table 2. P refers to the probable peak P–T conditions for the rock. Other explanations are the same as in Fig. 6.

measured in phengitic muscovite (3·26–3·28 p.f.u.) matches assemblages modeled at $P = 16{\cdot}4$–$18{\cdot}6$ kbar at $T = 553$°C in the H_2O-saturated assemblage gl–g–o–pa (Fig. 7a). However, equivalent isopleths of Si content in phengite extend to higher pressure conditions ($P > 20$ kbar) in the H_2O-absent assemblage gl–g–jd–pa, closer to the pressure estimates recovered from the garnet rim compositions.

Pseudosection for a garnet–glaucophane–albite schist (sample T316)

The NCKMnFMASHO P–T pseudosection calculated for the garnet–glaucophane–albite schist (sample T316) is presented in Fig. 8a. Compared with the pseudosections for the other two samples, there are much larger P–T ranges for jadeite- and albite-bearing equilibria as a result of elevated Na_2O content in the model bulk-rock composition. Pyrope and grossular contents measured in garnet reflect a more restricted P–T vector from 22·5 kbar at 532°C (point C, Fig. 8a) to maximum pressure conditions at 22·8 kbar and 543°C (point M, Fig. 8a), and peak conditions at 22 kbar and 550°C (point R, Fig. 8a) in the mineral assemblage gl–g–jd–pa–law. The Si content measured in phengite (3·30–3·32) is consistent with a similar pressure range of 21–23 kbar at $T = 540$–550°C. As in the other samples, mineral assemblages along this inferred prograde P–T vector are predicted to have evolved progressively through dehydration reactions. When the P–T vector moved to the boundary of lawsonite stability at $P \approx 22$ kbar, the rock is predicted to have had a H_2O content of 3·83 (mol %). Without fluid ingress, the post-peak decompression path would place the rock under fluid-absent conditions, entering the H_2O-absent assemblage gl–g–jd–pa (Fig. 8b). At $P \approx 14$ kbar, the transition from jadeite to albite would occur, and the hornblendic amphibole is

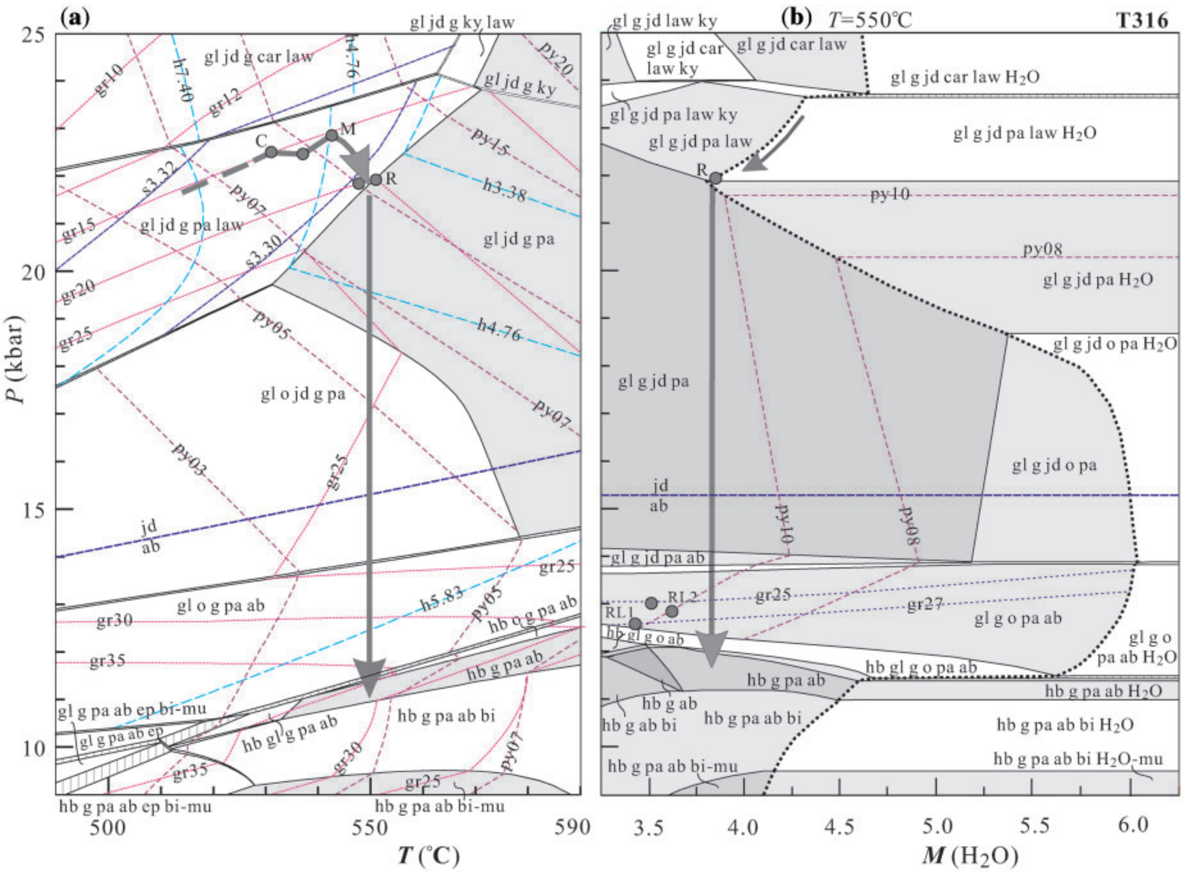

Fig. 8. (a) P–T pseudosection for sample T316 from the South Tianshan HP–UHP belt in the system NCKMnFMASHO (+ quartz + phengitic muscovite + H_2O) with a bulk composition calculated on the basis of normalized mole proportions as $SiO_2 = 67{\cdot}69$, $Al_2O_3 = 10{\cdot}90$, CaO $= 2{\cdot}78$, MgO $= 4{\cdot}67$, FeO $= 6{\cdot}00$, $K_2O = 0{\cdot}56$, $Na_2O = 7{\cdot}03$, MnO $= 0{\cdot}06$, O $= 0{\cdot}31$. (b) P–$M(H_2O)$ pseudosection at $T = 550$°C with quartz and phengitic muscovite in excess for sample T316. The bold dotted line in (b) refers to the H_2O saturation line. Projection of the garnet compositions is shown as dark grey circles with the labels C, M, R, RL1 and RL2 corresponding to those in Fig. 3 and Table 3. Other explanations are the same as in Fig. 6.

predicted to appear at $P \approx 12$ kbar. The grossular-rich rim compositions in garnet with $X_{py} \approx 0{\cdot}10$ and $X_{grs} = 0{\cdot}25$–$0{\cdot}27$ best match $P = 12{\cdot}5$–13 kbar in the H_2O-absent assemblage gl–g–o–pa–ab. The mineral assemblage observed in sample T316 has a H_2O content of *c.* 3·97 (mol %), only subtly higher than the $M(H_2O)$ predicted to have accompanied lawsonite breakdown (Fig. 8b).

DISCUSSION

Peak P–T estimates of the pelitic–felsic schists

The south Tianshan eclogite belt has extensive pelitic–felsic schists that enclose eclogite blocks. P–T estimates recovered from the eclogites provide critical context for the pelitic–felsic schists, to which common geothermobarometric techniques cannot be easily applied. The eclogite assemblages reflect $T = 500$–600°C on the basis of various versions of the garnet–omphacite thermometer and modeling using the P–T pseudosection approach, but pressure estimates vary widely (between 14 and 28 kbar) on the basis of barometers based on jadeite content in omphacite (Gao *et al.*, 1999), pseudosection approaches (Wei *et al.*, 2003) and the garnet–omphacite–phengite barometer (Klemd *et al.*, 2002; Zhang *et al.*, 2002a; Lin & Enami, 2006). Pressure estimates less then 20 kbar, based on the jadeite content in omphacite, are minimum estimates in the absence of albite (Carswell & Harley, 1990). In addition, the application of the pseudosection approach (Wei *et al.*, 2003) may have underestimated pressure conditions if the garnet and phengite compositions are not fully considered and the equilibration of mineral assemblages was incorrectly evaluated (Wei *et al.*, 2009). Generally, the garnet–omphacite–phengite barometers of Waters & Martin (1993) and Krogh Ravna & Terry (2004) yield pressure estimates for low-T eclogite assemblages considerably closer to the results recovered by modeling of garnet rim and phengite compositions on the P–T pseudosections (Wei *et al.*, 2009), although El-Shazly (2001) proposed that the garnet–omphacite–phengite barometer would overestimate pressure. Pressure estimates up to *c.* 28 kbar for the Tianshan eclogites are supported by the presence of UHP minerals such as coesite pseudomorphs, quartz and coesite exsolution lamellae in omphacite and magnesite (Zhang *et al.*, 2002*a*, 2002*b*, 2005). Thus, eclogite assemblages should reflect $P = 20$–28 kbar at $T = 500$–600°C.

P–T estimates for the widespread pelitic–felsic schists cluster in three distinct groups: *c.* 50 kbar at 560–600°C (Zhang *et al.* 2003), 27–33 kbar at 570–630°C (Lü *et al.*, 2008), and 14·5–16·5 kbar at 600–650°C (Wei & Powell, 2006). The present study on the three representative samples T311, T314 and T316 gives peak P–T estimates of *c.* 32 kbar at 550–570°C, *c.* 22·5 kbar at 553°C, and 22–23 kbar at 540–550°C, respectively. These conditions are consistent with the P–T estimates made using the eclogite assemblages. The ultrahigh-pressure estimate for sample T311 is supported by the presence of pseudomorphs after coesite in garnet and the discovery of coesite inclusions by Lü *et al.* (2008) in the intercalated rocks. The chloritoid inclusion in garnet in sample T314 is consistent with the presence of parageneses of chloritoid and glaucophane, or potentially also chloritoid and jadeite, supporting the low-T, high-P conditions constrained by the garnet growth zonation (Okay, 2002; Wei & Powell, 2006; Wei & Song, 2008).

Using the P–T pseudosection approach in the NCKFMASH system, Wei & Powell (2006) obtained a P–T estimate of 14·5–16·5 kbar and 600–650°C for sample AK07 by assuming that albite was in equilibrium with glaucophane, garnet and phengite. However, the garnet rim composition ($X_{py} = 0{\cdot}12$ and $X_{grs} = 0{\cdot}14$) and Si content in phengite (3·41–3·43 p.f.u.) best match equilibria modeled at 22–25 kbar at 550°C in the P–T pseudosection calculated for the sample, in good agreement with the above P–T estimates for the three samples discussed.

The South Tianshan eclogite belt is dominated by HP pelitic–felsic schists (22–25 kbar at 540–550°C), but contains UHP slices or blocks that recorded greater depths, although these HP and UHP rocks have not been well defined because of poor outcrop and difficult access. The pelitic–felsic schists seem most likely to be cofacial with the eclogite blocks, but experienced more extensive recrystallization during decompression.

Prograde *P*–*T* path from garnet zonation

Most garnet grains in the pelitic–felsic schists preserve extensive compositional zoning, involving core to rim increases in pyrope content coupled with constant or increasing grossular content. Some grains have pronounced ‘bell-shaped profiles’ in spessartine content, commonly interpreted to represent growth-dominated zoning (e.g. Spear, 1993). Using garnet isopleth thermobarometry, involving plotting compositional isopleths of garnet as contours on a P–T pseudosection (e.g. Zeh & Holness, 2003; Evans, 2004; Kim & Bell, 2005; Gaidies *et al.*, 2006; Le Bayon *et al.*, 2006; Wei & Song, 2008), prograde P–T paths were derived for the three Tianshan samples (Figs 6a, 7a and 8a). P–T conditions modeled from Si content in phengite are mostly in agreement with those constrained from garnet compositions. Garnet growth is interpreted to have occurred in mineral assemblages involving chloritoid, lawsonite, jadeite, coesite and potentially also carpholite, which are distinct from those now observed in the matrix. This focuses attention on implications drawn from the high-P phase equilibria modeling, but there are several points that support our interpretation of the prograde history: (1) chloritoid occurs as inclusions in garnet; (2) coesite has been reported from pelitic schist interlayered with rocks like sample T311 (Lü *et al.*, 2008) and probable pseudomorphs after coesite have been observed; (3) jadeite stability seems possible considering the extensive distribution of albite; (4) aggregates involving Fe-rich chlorite, grossular-rich garnet and epidote most probably reflect the presence of lawsonite and another ferromagnesian mineral in sample T314. Similar lawsonite pseudomorphs consisting of zoisite/epidote and paragonite have also been reported in the eclogite (Gao *et al.*, 1999). These observations suggest that the prograde path for the pelitic–felsic schists should have occurred within the stability fields of lawsonite, jadeite, chloritoid, and possibly carpholite or coesite. Phase equilibrium modeling can explain why these minerals might not survive, if the rocks were subjected to post-peak decompressional paths such as shown in Figs 6–8.

Post-peak decompression of the pelitic–felsic schist

The post-peak P–T paths are interpreted to have been controlled by decompression without pronounced cooling or heating (isothermal decompression; ITD) on the basis of late-stage garnet, albite and hornblendic amphibole, although the strictly ITD paths shown in Figs 6–8 are somewhat contrived. Two stages of decompression are inferred. During the early stage of decompression, mineral assemblage evolution is interpreted to have been controlled by dehydration related to the breakdown of the water-rich phases such as carpholite and lawsonite. At $T = 550$–560°C, all carpholite could be consumed through continuous reactions such as car + jd = pa + gl + law at 24–25 kbar, and lawsonite subsequently consumed through continuous reactions such as law + jd = gl + pa + ep at 20–22 kbar. During this early decompression, the modal proportions of glaucophane and paragonite are predicted to have increased at the expense of jadeite, and the compositions of the outer rims of garnet grains may have been modified (such as in samples T314 and 316) with the observed rim compositions closely matching those predicted for the lawsonite-out line. However, in some samples such as T311, garnet growth zonation is well preserved. The Si content in phengite mostly reflects pressure conditions at the metamorphic peak or early stage decompression.

Following the breakdown of lawsonite, further isothermal decompression, without fluid ingress, is predicted to have led to water-absent conditions in the Tianshan samples from the contours of the H_2O isopleths in the pseudosections. Under such fluid-absent conditions, albite replaces jadeitic omphacite at $P \approx 14$ kbar, and hornblendic amphibole appears at $P = 12-13$ kbar, distinct from the water-saturated conditions where albite is usually stable at much lower pressure conditions (Figs 6b and 7b). It seems that a solid transition from jadeitic pyroxene to albite could have occurred under these fluid-absent conditions, although this process might have been catalyzed by the presence of fluid (Holland, 1980). From this point of view, it is reasonable to conclude that most of the albite, especially the albite poikiloblasts that have inclusions of glaucophane, rutile, phengite and paragonite, could be interpreted as the products of jadeite breakdown, although this interpretation has been criticized by El-Shazly (2001).

The late-stage garnet with high grossular and low pyrope contents could be modeled to have coexisted with albite, hornblendic amphibole and glaucophane under the H_2O-absent conditions. The present water contents of the three Tianshan samples are similar to, or only subtly higher than those predicted for lawsonite breakdown, but apparently lower than the values of water saturation under conditions of 12–13 kbar for the stability of hornblendic amphibole and albite. This is consistent with limited water infiltration having occurred, which favors the preservation of early stage assemblages and also the formation of albite.

Retrogression of the HP–UHP pelitic–felsic schists and gneisses

In many HP–UHP terranes (e.g. Western Gneiss Region, Norway; Dabie Shan, China; Dora Maira Massif, Western Alps; Adula Nappe, Central Alps; Erzgebirge, Bohemian Massif), the post-peak retrogression is more intense in pelitic–felsic schists and gneisses than in the enclosed mafic eclogites (e.g. Cuthbert & Carswell, 1990; Wang *et al.*, 1990; Schertl *et al.*, 1991; Schmadike *et al.*, 1992). This phenomenon is commonly attributed to either (1) retrograde reactions in pelitic–felsic rocks releasing fluids upon depressurization, whereas mafic rocks require fluids for retrogression (e.g. Heinrich, 1982; Auzanneau *et al.*, 2006) or (2) retrograde reactions in pelitic–felsic rocks being kinetically faster than the equivalent reactions in mafic rocks (e.g. Schreyer, 1995). The experimental study of Auzanneau *et al.* (2006) has shown that the transition of felsic eclogitic rocks into amphibolite-facies assemblages under suprasolidus conditions ($T = 800–900°C$) would release fluid-rich melts through the phengite dehydration melting reaction phengitic muscovite + omphacite + quartz = biotite + plagioclase + garnet + melt. Generally, the melt- (or fluid)-releasing progressive reactions are interpreted to easily reach an equilibrium state, resulting in intensive obliteration of the early mineral assemblages (Guiraud *et al.*, 2001; White *et al.*, 2001). Moreover, the migration and crystallization of such melts could trigger the retrogression of the mafic eclogites. Thus, the HP–UHP pelitic–felsic rocks should have been intensively or completely replaced by lower pressure assemblages during decompression at temperatures above the solidus if the rocks contained phengite in the peak stage. These pelitic–felsic rocks do not require fluid infiltration for their decompressional changes, distinct from the retrogression of mafic eclogite assemblages.

Decompression of the HP–UHP pelitic–felsic rocks under subsolidus conditions as shown in Figs 6–8 can be divided into two stages. The early stage is dominated by the dehydration of carpholite and lawsonite, resulting in considerable changes in the mineral assemblage and compositions. The later-stage decompression after lawsonite disappears is characteristic of fluid-absent conditions. With the exception of the solid-state transition of jadeite to albite, the HP–UHP assemblages tend to be preserved. During this subsolidus decompression the phengitic muscovite remains stable and commonly keeps the compositions of peak or early decompression stages until it transforms into biotite at lower pressures.

Tectonic implications

The South Tianshan HP–UHP belt has been interpreted to have formed by the northward subduction of Paleozoic south Tianshan oceanic crust (Gao *et al.*, 1998; Gao & Klemd, 2003). Mafic eclogites with OIB, enriched (E)-MORB and normal (N)-MORB affinities represent basalts formed at seamount settings within the ocean. Similar to the evolution of 'Cordilleran-type' blueschists formed by oceanic subduction (Maruyama *et al.*, 1996), these basalts were dismembered and intermingled with greywackes within an accretionary wedge during the continuous subduction of oceanic crust. The present study has suggested that both the seamount basalts and greywacke sediments were subducted to depths of 70–100 km, and returned from these depths to the surface.

Using the thermodynamic dataset of Holland & Powell (1998), densities calculated for samples T314 and T316 are $2·93–3·03$ g/cm^3 at $P–T$ conditions of 23 kbar and 550°C, and $3·08$ g/cm^3 for sample T311 at 32 kbar and 560°C. At the same $P–T$ conditions, the density calculated for eclogite of MORB composition ranges from 3·25 to 3·31 g/cm^3, similar to or somewhat denser than the mantle rocks at the same depth (Hermann, 2002). Thus, the subducted sediments are buoyant at mantle depths and this might provide a driving force for fast exhumation of the HP–UHP rocks, especially the enclosing eclogite blocks (Platt, 1993; Rubatto & Hermann, 2001). The post-peak $P–T$ paths of the South Tianshan eclogites and pelitic–felsic schists involved near-isothermal decompression (see Figs 6–8 and Gao & Klemd, 2003), indicating that these rocks were rapidly and adiabatically uplifted to a lower crustal level and recrystallized at epidote- to amphibolite-facies conditions. The subsequent exhumation of the South Tianshan HP–UHP rocks from the lower crust is inferred to have resulted from large-scale thrusting in the later stage of collision (Gao *et al.*, 1998), accompanied by an overprint of greenschist-facies metamorphism.

Most oceanic subduction-related HP accretionary terranes around the world are dominated by felsic–pelitic metasediments. Buoyancy of the subducted metasediments with respect to mantle rocks could be one of the major reasons for rapid exhumation of such HP terranes.

CONCLUSIONS

Pelitic–felsic schist assemblages, which are prevalent in most oceanic subduction-related HP accretionary terranes but are mostly poorly studied because of lack of available geothermobarometric techniques, can be well modeled using the pseudosection approach. Contours of composition isopleths for minerals such as garnet and phengite can be used to derive prograde and retrograde P–T paths of metamorphism. Pelitic–felsic schists in the South Tianshan HP–UHP belt recorded peak P–T conditions of 22–32 kbar and 540–570°C, consistent with the P–T estimates recovered from eclogite blocks enclosed in the schists. A post-peak decompression is interpreted to have involved two stages: an early stage decompression characterized by dehydration reactions mainly involving carpholite and lawsonite breakdown, and a subsequent decompression controlled by fluid-absent conditions. Fluid-absent conditions favor the preservation of early stage minerals, and the solid transition of jadeite to albite at higher pressures than would occur in fluid-saturated conditions. Decompression of the pelitic–felsic rocks at sub-solidus conditions did not destabilize early phengitic muscovite, which records high-P conditions in the absence of a pronounced fluid infiltration. The pelitic–felsic schists and the enclosing eclogite blocks in the South Tianshan HP–UHP belt share cofacial metamorphic evolutional histories. The subducted metasediments might provide a driving force for fast exhumation of the HP–UHP rocks.

ACKNOWLEDGEMENTS

This work was financially supported by the National Natural Science Foundation of China (Grant numbers 40730314 and 40525006). W.W. acknowledges the support of an Endeavor Post-graduate International Research Scholarship at the University of Sydney.

REFERENCES

Ai, Y., Zhang, L. F., Li, X. P. & Qu, J. F. (2005). The geochemical characteristics and tectonic implications of the UHP eclogites and blueschists, Southwestern Tianshan, China. *Progress in Natural Science* **11**, 1346–1356 (in Chinese with English abstract).

Allen, M. B., Windley, B. F. & Zhang, C. (1992). Paleozoic collisional tectonics and magmatism of the Chinese Tien Shan, central Asia. *Tectonophysics* **220**, 89–115.

Auzanneau, E., Vielzeuf, D. & Schmidt, M. W. (2006). Experimental evidence of decompression melting during exhumation of subducted continental crust. *Contributions to Mineralogy and Petrology* **152**, 125–148.

Carson, C. J., Powell, R. & Clarke, G. L. (1999). Calculated mineral equilibria for eclogites in CaO–Na_2O–FeO–MgO–Al_2O_3–SiO_2–H_2O: application to the Pouébo Terrane, Pam Peninsula, New Caledonia. *Journal of Metamorphic Geology* **17**, 9–24.

Carswell, D. A. & Harley, S. L. (1990). Mineral barometry and thermometry. In: Carswell, D. A. (ed.) *Eclogite Facies Rocks*. Glasgow: Blackie, pp. 83–110.

Carswell, D. A. & Zhang, R. Y. (2000). Petrographic characteristics and metamorphic evolution of ultrahigh-pressure eclogites in the plate-collision belts. In: Ernst, W. G. & Liou, J. G. (eds) *Ultra-high Pressure Metamorphism and Geodynamics in Collision-type Orogenic Belts*. Columbia, MD: Bellwether, pp. 39–56.

Clarke, G. L., Powell, R. & Fitzherbert, J. A. (2006). The lawsonite paradox: a comparison of field evidence and mineral equilibria modeling. *Journal of Metamorphic Geology* **24**, 716–726.

Coggon, R. & Holland, T. J. B. (2002). Mixing properties of phengitic micas and revised garnet–phengite thermobarometers. *Journal of Metamorphic Geology* **20**, 683–696.

Coleman, R. G. (1989). Continental growth of Northwest China. *Tectonics* **8**, 621–635.

Cuthbert, S. J. & Carswell, D. A. (1990). Formation and exhumation of medium-temperature eclogites in the Scandinavian Caledonides. In: Carswell, D. A. (ed.) *Eclogite Facies Rocks*. Glasgow: Blackie, pp. 180–203.

Diener, J. F. A., Powell, R., White, R. W. & Holland, T. J. B. (2007). A new thermodynamic model for clino- and orthoamphiboles in the system Na_2O–CaO–FeO–MgO–Al_2O_3–SiO_2–H_2O–O. *Journal of Metamorphic Geology* **25**, 631–656.

El-Shazly, A. K. (2001). Are pressures for blueschists and eclogites overestimated? The case from NE Oman. *Lithos* **56**, 231–264.

El-Shazly, A. K. & Liou, J. G. (1991). Glaucophane chloritoid-bearing assemblages from NE Oman: petrologic significance and a petrogenetic grid for high-P metapelites. *Contributions to Mineralogy and Petrology* **107**, 180–201.

Evans, T. P. (2004). A method for calculating effective bulk composition modification due to crystal fractionation in garnet-bearing schist: implications for isopleth thermobarometry. *Journal of Metamorphic Geology* **22**, 547–557.

Gaidies, F., Abart, R., De Capitani, C., Schuster, R., Connolly, J. A. D. & Reusser, E. (2006). Characterization of polymetamorphism in the Austroalpine basement east of the Tauern Window using garnet isopleths thermobarometry. *Journal of Metamorphic Geology* **24**, 451–476.

Gao, J. & Klemd, R. (2003). Formation of HP–LT rocks and their tectonic implications in the western Tianshan Orogen, NW China: geochemical and age constraints. *Lithos* **66**, 1–22.

Gao, J., He, G., Li, M., Xiao, X., Tang, Y., Zhou, M. & Wang, J. (1995). The mineralogy, petrology, metamorphic PTDt trajectory and exhumation mechanism of blueschists, south Tianshan, northwestern China. *Tectonophysics* **250**, 151–168.

Gao, J., Li, M., He, G., Xiao, X. & Tang, Y. (1998). Paleozoic tectonic evolution of the Tianshan Orogen, northwestern China. *Tectonophysics* **287**, 213–231.

Gao, J., Klemd, R., Zhang, L., Wang, Z. & Xiao, X. (1999). *P–T* path of high-pressure/low-temperature rocks and tectonic implications in the western Tianshan Mountains, NW China. *Journal of Metamorphic Geology* **17**, 621–636.

Green, E. C. R., Holland, T. J. B. & Powell, R. (2007). An order–disorder model for omphacitic pyroxenes in the system jadeite–diopside–hedenbergite–acmite, with applications to eclogitic rocks. *American Mineralogist* **92**, 1181–1189.

Guiraud, M., Powell, R. & Rebay, G. (2001). H_2O in metamorphism and unexpected behavior in the preservation of metamorphic mineral assemblages. *Journal of Metamorphic Geology* **19**, 445–454.

Heinrich, C. A. (1982). Kyanite eclogite to amphibolite facies evolution of hydrous mafic and pelitic rocks, Adula Nappe, Central Alps. *Contributions to Mineralogy and Petrology* **81**, 30–38.

Hermann, J. (2002). Experimental constraints on phase relations in subducted continental crust. *Contributions to Mineralogy and Petrology* **143**, 219–235.

Holland, T. J. B. (1980). The reaction albite = jadeite + quartz determined experimentally in the range 600–1200°C. *American Mineralogist* **65**, 129–134.

Holland, T. J. B. & Powell, R. (1996). Thermodynamics of order–disorder in minerals: II. Symmetric formalism applied to solid solutions. *American Mineralogist* **81**, 1425–1437.

Holland, T. J. B. & Powell, R. (1998). An internally consistent thermodynamic data set for phases of petrological interest. *Journal of Metamorphic Geology* **16**, 309–343.

Holland, T., Barker, J. & Powell, R. (1998). Mixing properties and activity–composition relationships of chlorites in the system $MgO–FeO–Al_2O_3–SiO_2–H_2O$. *European Journal of Mineralogy* **10**, 395–406.

Jahn, B.-m., Liu, X., Yui, T., Morin, N. & Coz, M. B. -l. (2005). High pressure/ultrahigh-pressure eclogites from the Hong'an Block, East–Central China: geochemical characterization, isotope disequilibrium and geochronological controversy. *Contributions to Mineralogy and Petrology* **149**, 499–526.

Kelly, S., Arnaud, N. & Okay, A. (1994). Anomalously old Ar–Ar ages in high-pressure metamorphic terrains. *Mineralogical Magazine* **58**, 468–469.

Kim, H. S. & Bell, T. H. (2005). Combining compositional zoning and foliation intersection axes (FIAs) in garnet to quantitatively determine early *P–T–t* paths in multiply deformed and metamorphosed schists: north central Massachusetts, USA. *Contributions to Mineralogy and Petrology* **149**, 141–163.

Klemd, R., Schröter, F. C., Will, T. M. & Gao, J. (2002). *P–T* evolution of glaucophane–omphacite bearing HP–LT rocks in the western Tianshan Orogen, NW China: new evidence for 'Alpine-type' tectonics. *Journal of Metamorphic Geology* **20**, 239–254.

Krogh Ravna, E. J. & Terry, M. P. (2004). Geothermobarometry of UHP and HP eclogites and schists—an evaluation of equilibria among garnet–clinopyroxene–kyanite–phengite–coesite/quartz. *Journal of Metamorphic Geology* **22**, 579–592.

Leake, B. E., Woolley, A. R., Arpes, C. E. S. *et al*. (1997). Nomenclature of amphiboles: report of the Subcommittee on amphiboles of the International Mineralogical Association, Commission on New Minerals and Mineral Names. *American Mineralogist* **82**, 1019–1037.

Le Bayon, B., Pitra, P., Ballevre, M. & Bohn, M. (2006). Reconstructing *P–T* paths during continental collision using multi-stage garnet (Gran Paradiso nappe, western Alps). *Journal of Metamorphic Geology* **24**, 477–496.

Li, Q. & Zhang, L. F. (2004). The *PT* path and geological significance of low-pressure granulite-facies metamorphism in Muzhaerte, southwest Tianshan, Xinjiang, China. *Acta Petrologica Sinica* **20**, 583–594 (in Chinese with English abstract).

Li, S., Wang, S., Chen, Y., Zhou, H., Zhang, Z., Liou, G. & Qiou, J. (1994). Excess argon in phengite of eclogite: evidence from comparing dating of eclogite by Sm–Nd, Rb–Sr, and $^{40}Ar/^{39}Ar$ isotope methods. *Chemical Geology* **112**, 343–350.

Lin, W. & Enami, M. (2006). Prograde pressure–temperature path of jadeite-bearing eclogites and associated high-pressure/low-temperature rocks from western Tianshan, northwest China. *Island Arc* **15**, 483–502.

Lü, Z., Zhang, L. F., Du, J. X. & Bucher, K. (2008). Coesite inclusions in garnet from eclogitic rocks in western Tianshan, northwest China: convincing proof of UHP metamorphism. *American Mineralogist* **93**, 1845–1850.

Marmo, B., Clarke, G. L. & Powell, R. (2002). Fractionation of bulk rock composition due to porphyroblast growth: effects on eclogite facies mineral equilibria, Pam Peninsula, New Caledonia. *Journal of Metamorphic Geology* **20**, 151–165.

Maruyama, S., Liou, J. G. & Terabayashi, M. (1996). Blueschists and eclogites of the world and their exhumation. *International Geological Reviews* **38**, 485–594.

Miyazaki, K., Zulkarnain, I., Sopaheluwakan, J. & Wakita, K. (1996). Pressure–temperature conditions and retrograde paths of eclogites, garnet glaucophane rocks and schists from South Sulawesi, Indonesia. *Journal of Metamorphic Geology* **14**, 549–563.

Okay, A. I. (2002). Jadeite–chloritoid–glaucophane–lawsonite blueschists in northwestern Turkey: unusually high *P/T* ratios in continental crust. *Journal of Metamorphic Geology* **20**, 757–768.

Patrick, B. E. & Evans, B. W. (1989). Metamorphic evolution of the Seward Peninsula blueschist terrane. *Journal of Petrology* **30**, 531–555.

Platt, J. P. (1993). Exhumation of high pressure rocks: a review of concepts and processes. *Terra Nova* **5**, 119–133.

Powell, R. (1978). *Equilibrium Thermodynamics in Petrology (an Introduction)*. London: Harper & Row, 284 pp.

Powell, R. & Holland, T. J. B. (1999). Relating formulations of the thermodynamics of mineral solid solutions: Activity modeling of pyroxenes, amphiboles, and micas. *American Mineralogist* **84**, 1–14.

Powell, R. & Holland, T. J. B. (2008). On thermobarometry. *Journal of Metamorphic Geology* **26**, 155–179.

Powell, R., Holland, T. & Worley, B. (1998). Calculating phase diagram involving solid solutions via non-linear equations, with examples using THERMOCALC. *Journal of Metamorphic Geology* **16**, 577–586.

Schertl, H. P., Schreyer, W. & Chopin, C. (1991). The pyrope–coesite rocks and their country rocks at Parigi, Dora Maira Massif, Western Alps: detailed petrography, mineral chemistry and *PT*-path. *Contributions to Mineralogy and Petrology* **108**, 1–21.

Schmadike, E., Okrusch, M. & Schmidt, W. (1992). Eclogite facies rocks in the Saxonian Erzgebirge, Germany: high pressure metamorphism under contrasting *P–T* conditions. *Contributions to Mineralogy and Petrology* **110**, 226–241.

Schreyer, W. (1995). Ultradeep metamorphic rocks: the retrospective viewpoint. *Journal of Geophysical Research* **100**(B5), 8353–8366.

Sobolev, N. V., Dobretsov, N. L., Bakirov, A. B. & Shatsky, V. S. (1986). Eclogites from various types of metamorphic complexes in the USSR and the problems of their origin. In: Evans, B. W. & Brown, E. H. (eds.) *Blueschists and Eclogites. Geological Society of America, Memoirs* **164**, 349–363.

Song, S. G., Zhang, L. F., Niu, Y. L., Wei, C. J., Liou, J. G. & Shu, G. M. (2007). Eclogite and carpholite-bearing meta-pelite in the North Qilian suture zone, NW China: implications for Paleozoic oceanic subduction. *Journal of Metamorphic Geology* **25**, 547–563.

Spear, F. S. (1993). *Metamorphic Phase Equilibria and Pressure–Temperature–Time Paths. Mineralogical Society of America, Monograph*, 799 pp.

Stüwe, K. (1997). Effective bulk composition changes due to cooling: a model predicting complexities in retrograde reaction textures. *Contributions to Mineralogy and Petrology* **129**, 43–52.

Rubatto, D. & Hermann, J. (2001). Exhumation as fast as subduction? *Geology* **29**, 3–6.

Tagiri, M., Yano, T., Bakirov, A., Nakajima, T. & Uchiumi, S. (1995). Mineral parageneses and metamorphic P–T paths of ultrahigh-pressure eclogites from Kyrghyzstan Tien-Shan. *Island Arc* **4**, 280–292.

Thurston, S. P. (1985). Structure, petrology and metamorphic history of the Nome Group blueschist terranes, Salmon Lake area, Seward Peninsula, Alaska. *Geological Society of America Bulletin* **96**, 600–617.

Tinkham, D. K. & Ghent, E. D. (2005). Estimating P–T conditions of garnet growth with isochemical phase-diagram sections and the problem of effective bulk-composition. *Canadian Mineralogist* **43**, 35–50.

Tracy, R. J. (1982). Compositional zoning and inclusions in metamorphic minerals. In: Ferry, J. M. (ed.) *Characterization of Metamorphism through Mineral Equilibria. Mineralogical Society of America, Reviews in Mineralogy* **10**, 355–397.

Vance, D. & Holland, T. J. B. (1993). A detailed isotopic and petrological study of a single garnet from the Gassetts Schist, Vermont. *Contributions to Mineralogy and Petrology* **114**, 101–118.

Volkova, N. I. & Budanov, V. I. (1999). Geochemical discrimination of metabasalt rocks of the Fan–Karategin transitional blueschist/greenschist belt, South Tianshan, Tajikistan: seamount volcanism and accretionary tectonics. *Lithos* **47**, 201–216.

Wang, X., Jing, Y., Liou, J. G., Pan, G., Liang, W., Xia, M. & Maruyama, S. (1990). Field occurrences and petrology of eclogites from the Dabie Mountains, Anhui, central China. *Lithos* **25**, 119–131.

Warren, C. J. & Waters, D. J. (2006). Oxidized eclogites and garnet–blueschists from Oman: P–T path modeling in the NCFMASHO system. *Journal of Metamorphic Geology* **24**, 783–802.

Waters, D. J. & Martin, H. N. (1993, updated 1996). Geobarometry of phengite-bearing eclogites. *Terra Abstracts* 5, 410–411.

Wei, C. J. & Powell, R. (2004). Calculated phase relations in high-pressure metapelites in the system NKFMASH (Na_2O–K_2O–FeO–MgO–Al_2O_3–SiO_2–H_2O) with application to natural rocks. *Journal of Petrology* **44**, 183–202.

Wei, C. J. & Powell, R. (2006). Calculated phase relations in the system NCKFMASH (Na_2O–CaO–K_2O–FeO–MgO–Al_2O_3–SiO_2–H_2O) for high-pressure metapelites. *Journal of Petrology* **47**, 385–408.

Wei, C. J. & Song, S.G. (2008). Chloritoid–glaucophane schist in the north Qilian orogen, NW China: phase equilibria and P–T path from garnet zonation. *Journal of Metamorphic Geology* **26**, 301–316.

Wei, C. J., Powell, R. & Zhang, L. F. (2003). Eclogites from the south Tianshan, NW China: petrologic characteristic and calculated mineral equilibria in the Na_2O–CaO–FeO–MgO–Al_2O_3–SiO_2–H_2O system. *Journal of Metamorphic Geology* **21**, 163–179.

Wei, C. J., Powell, R. & Clarke, G. L. (2004). Calculated phase equilibria for low- and medium-pressure metapelites in the KFMASH and KMnFMASH systems. *Journal of Metamorphic Geology* **22**, 495–508.

Wei, C. J., Yang, Y., Su, X. L., Song, S. G. & Zhang, L. F. (2009). Metamorphic evolution of low-T eclogite from the north Qilian orogen, NW China: Evidence from petrography and calculated phase equilibria in system NCKFMASHO. *Journal of Metamorphic Geology* **27**, 55–70.

White, R. W., Powell, R. & Holland, T. J. B. (2001). Calculation of partial melting equilibria in the system Na_2O–CaO–K_2O–FeO–MgO–Al_2O_3–SiO_2–H_2O (NCKFMASH). *Journal of Metamorphic Geology* **19**, 139–153.

White, R. W., Powell, R. & Clarke, G. L. (2003). Prograde metamorphic assemblage evolution during partial melting of metasedimentary rocks at low pressures: migmatites from Mt Stafford, Central Australia. *Journal of Petrology* **44**, 1937–1960.

Windley, B. F., Allen, M. B., Zhang, C., Zhao, Z.-Y. & Wang, G.-R. (1990). Paleozoic accretion and Cenozoic redeformation of the Chinese Tian Shan range, Central Asia. *Geology* **18**, 129–131.

Zeh, A. & Holness, M. B. (2003). The effect of reaction overstep on garnet microtextures in metapelitic rocks on the Ilesha Schist Belt, SW Nigeria. *Journal of Petrology* **44**, 967–994.

Zhang, L. F., Gao, J., Aikebel & Wang, Z. (2000). Metamorphism of low-temperature eclogites in western Tianshan, Xinjiang. *Science in China (D)* **30**, 345–354 (in Chinese).

Zhang, L. F., Ellis, D. J. & Jiang, W. (2002*a*). Ultrahigh pressure metamorphism in western Tianshan, China, part I: evidences from the inclusion of coesite pseudomorphs in garnet and quartz exsolution lamellae in omphacite in eclogites. *American Mineralogist* **87**, 853–860.

Zhang, L. F., Ellis, D. J., Williams, S. & Jiang, W. (2002*b*). Ultrahigh pressure metamorphism in western Tianshan, China, part II: evidence from magnesite in eclogite. *American Mineralogist* **87**, 861–866.

Zhang, L. F., Ellis, D. J., Arculus, R. J., Jiang, W. & Wei, C. J. (2003). 'Forbidden zone' subduction of sediments to 150 km depth—the reaction of dolomite to magnesite + aragonite in the UHPM metapelites from western Tianshan, China. *Journal of Metamorphic Geology* **21**, 523–529.

Zhang, L. F., Song, S. G., Ai, Y. L. & Liou, J. G. (2005). Relict coesite exsolution in omphacite from western Tianshan eclogites, China. *American Mineralogist* **89**, 180–186.

Zhang, L. F., Ai, Y., Song, S. G., Song, B., Rubatto, D., Williams, S., Liou, J. G. & Ellis, D. (2007). Triassic collision of Western Tianshan orogenic belt, China: evidences from SHRIMP U–Pb dating of zircon from eclogitic rocks. *Lithos* **96**, 266–280.